Development novel collision approach for particulate flows

Wojciech Adamczyk (wojciech.adamczyk@polsl.pl)
Silesian University of Technology https://orcid.org/0000-0002-9178-9566
Agata Widuch
Silesian University of Technology
Pawel Morkisz
AGH University of Science and Technology
Kari Myohanen
Lappeenranta-Lahti University of Technology LUT
Adam Klimanek
Silesian University of Technology
Sebastian Pawlak
Silesian University of Technology

Article

Keywords: multiphase flows, particle tracking, machine learning, particle collision, surrogate model, CFD

Posted Date: October 28th, 2022

DOI: https://doi.org/10.21203/rs.3.rs-2178782/v1

Development novel collision approach for particulate flows

Agata Widuch[a], Pawel Morkisz[c], Kari Myöhänen[b], Adam Klimanek[a], Sebastian Pawlak[a,d], Wojciech Adamczyk[a,*]

[a] *Silesian University of Technology, Faculty of Energy and Environmental Engineering, Department of Thermal Engineering, Konarskiego 22, 44-100 Gliwice, Poland*
[b] *Lappeenranta-Lahti University of Technology LUT, LUT School of Energy Systems, P.O. Box 20, FI-53851 Lappeenranta, Finland*
[c] *AGH University of Science and Technology, Faculty of Applied Mathematics, Al. Mickiewicza 30, 30–059 Krakow, Poland*
[d] *Silesian University of Technology, Faculty of Mechanical Engineering, Scientific and Didactic Laboratory of Nanotechnology and Materials Technologies, Towarowa 7A, 44-100 Gliwice, Poland*

Abstract

With technology development, there is a growing need for an accurate simulation tools, allowing the best possible representation of the reality. Developed model found not only application in prototyping process but can provide significant knowledge into the artificial intelligent model extending their comprehension. Computational performance and accuracy of the numerical model, dedicated for granular flows are mostly a function of mathematical model that track the mutual interaction between particles. Currently the kinetic theory of granular flow or soft- and hard-sphere collision models are used for modeling particle interactions. Each of them suffers from some imperfection that often limit the problem sizes. The purpose of this work is building new mathematical approach, not only fast, but also accurate regarding predicting collisions and determining particle trajectories by application of machine learning technique.

Keywords: multiphase flows, particle tracking, machine learning, particle collision, surrogate model, CFD

*Corresponding author: Wojciech Adamczyk wojciech.adamczyk@polsl.pl

October 25, 2022

1. Introduction

Flows, where the particulate interactions are predominant are present not only in various industries but also in the nature and bioengineering. Very good representative of such flows is transport of reed blood cells (RBC) as the oxygen carrier. For instance, [1] experimentally studied the persistent effect of the red blood cells retain their ability to move in microcapillaries under high levels of oxidative stress or [2] used granular model for tracking and cell-free layer formation of RBCs in a microchannel with hyperbolic contraction.

. Development of accurate and robust model capable to efficiently model RBC is desirable to add new knowledge to experimental data. An industry example can be found in the fluidization phenomenon [3] used in energy sector, food processing [4], emptying of large silos [5] in agricultural facilities or in case of modeling avalanches [6].

Nevertheless, due to the complexity of the physic that stands behind such flows the available mathematical models still require significant improvements [7, 8] to be wider used for more sophisticated, basic sciences applications as discussed [9].Dense granular flows, are characterized by significant interactions between particles and solid—gaseous phases [10]. The application of the computational fluid dynamics (CFD) to simulate this type flows are not a trivial task, either in industrial or on a laboratory scales. Currently available and frequently used approaches, for modeling particulate transport, are the two-fluid Euler-Euler (EE) approach [11], hybrid Eulerian-Lagrangian (HEL) [12, 13, 14, 15], and Discrete Element Method (DEM) [16, 17, 18]. The main differences between these approaches are related to the implementation of mathematical models dedicated for modeling collisions between particles. The first two approaches use the Kinetic Theory of Granular Flow (KTGF) [19, 20], to predict the common particle interaction in the solid phase. The last one uses hard- or soft-sphere models [18, 21] to track particle collisions, where direct particle-particle interactions are recognized.

By application of the EE or HEL approach the collision forces that acts on the particles are determined based on the volume fraction of the solid material in computational cell according mentioned KTGF theory [22]. The accuracy of this technique is strongly related to the mesh resolution, where the particle properties are average over computational cell. There are some techniques to increase these models accuracy by application of the energy minimum multi-scale method (EMMS) [23, 24]. This model affects the predicted drag force, that acts on the solid phase, thereby the prediction of the solid phase distribution, that affects collision [25].

The main feature, that excludes the DEM model from the large-scale application, is the unprofitably long computation time [26]. This model spatially and temporally tracks individually each of the particle stored in the system, which affects the simulation time. Depending on the number of particles in the computational domain, the time can stretch from hours to days of simulation. In many cases, this is an unacceptable time, despite its accuracy. Furthermore, the huge difference between the DEM approach and the HEL technique [27] is related to the way, how the solid particles are tracked. By application of the HEL approach the idea of individual particle tracking is replaced by introducing the principle of particle grouping in to parcels. Each parcel stores particles with the same physical properties [12], i.e. velocity, temperature, mass, size. This approach considerably reduces cost of numerical simulation, which allows for its application for solving industrial scale problems. Nevertheless, some implementation of the DEM allows similar future while this leads for not physical distribution of the particles due to problems, with accurate representation of the mathematical model closure terms.

Knowing the basic advantages and disadvantages of the above-mentioned approaches used for modeling dense granular flows, it is straightforward that there is a real need to develop the model that can combine aforementioned advantages of each model. The question arise, how the accurate DEM collision model can be combined with the simple HEL technique. Presented work deals with it, by introduction of a novel collision model to the standard HEL approach, which goal was to replace the KTGF theory for determination collision force. Developed model keeps the accuracy of the DEM but significantly decreases the computational time. it was reached by introduction of reduced order model (ROM) built in the frame of the machine learning algorithms, to become a surrogate collision model.

Nowadays, the machine learning (ML) became increasingly popular in number of different industrial applications, i.e. drug discovery and development [28], marine to optimize power and fuel consumption during ship transportation [29], for modeling optimizing of complex process [30, 31, 21, 32], application in modeling and

performance analysis of ocean robots [33], for prediction of a battery storage [34], interval for wind power forecasting [35] and forecasting the crude oil prices [36, 37]. Application of the ML has a very high level of accuracy, but most importantly allows results to be obtained in a very short time in case of usage of the ML as ROMs. The ML technique is getting popular in field of development ROM to reduce computational cost. An example of the physics-informed machine learning for reduced-order modeling can be found in [38]. Very applicable work, focused on application of the ROM technique, for modeling furnace operation in flameless conditions in terms of the digital twin concept can be found in [39]. Other interesting work, that goal is to apply the ROM for representation of the redox kinetics of the oxygen carrier in chemical looping combustion can be found in [40]. All aforementioned works, show the applicability of the ML algorithm is seen as very powerfully tools that have huge potential in reduction cost of numerical simulation.

The activities in this work were divided into two phases: firstly the novel collision/surrogate model in terms of the ML technique was developed applying accurate DEM approach. Once it was done, the developed surrogate collision model (SCM) was implemented into the solution procedure of the standard HEL technique to replace the KTGF. Developed SCM was implemented into the solution procedure through the set of user defined functions (UDFs). Within the second stage, the Hybrid Euler-Lagrange Surrogate Collision Model (HELSCM) results, were juxtaposed with numerical results obtained by application of standard HEL and DEM approaches, using the solid phase velocity profiles. The required data for experimental work was extracted using in-house tracking algorithm described in [41], while for numerical data processing the UDFs were used. Additionally, to check behavior of the HELSCM approach, the quantitative comparison was made, based on observation particles/parcels distribution during numerical simulations. For that purpose two particle sizes were used, i.e. 315 μm and 475 μm, where for quantitative comparison the solid velocity profiles were used obtained from carried out experimental work.

Developed HELSCM model showed that numerical results were consistent with those collected during experimental work. The advantages of the introduced methodology is the possibility of modeling multiphase flow, with particle distribution, in the level of accuracy of the DEM approach, with the time step order as used in case of application standard HEL technique. In case of using the standard DEM, the simulation time step is a function of the flow conditions, and can be even smaller than 10^{-5} s. In such case, the simulation time can by considerably higher than that reached by application of developed HELSCM model.

2. Experimental test rig

The experimental test rig used for measurements, is located at the Silesian University of Technology in the Department of Thermal Engineering laboratory. A detailed description, of the experimental facility was discussed in [41], while the simplified sketch is presented in figure 1. The main components of the device are the transparent core, the side arms, and the air distribution system. Air, at a specific volumetric flow rate controlled by Bronkhorst HIGH-TECH B.V. [42] flow controllers, is supplied through air inlets. Once the flow is stabilized, particles are released from the particle holders and introduced through the arms into the particle collision region. To capture the collisions and trajectory of particles, the high speed camera VEO 710L [43] equipped with a NIKKOR 200 mm F/4.0 MACRO lens, was used. The used image resolution was 1280x720 and the frame rate of recorded images was set to 8300 frames per second (fps).

With selected image resolution 1280x720 (reduced in contrary to the previous work [41]) and selected configuration of the the camera in respect to test-rig; it was possible to obtain field of view that covers particle collision region (see Fig. 1), together with particle inlets. Figure 1 illustrates the space location of the ten boxes used for determination of the particle velocity profiles. To determine the particle velocity profiles in specified locations, an in-house algorithm developed within the framework of the LabVIEW (National Instruments Corp., USA) [44] application was used, in combination with Python script for data processing. The detailed description about algorithm functionality can be found [41].

As the material for testing, a polyethylene microsphere particles with a density of 1000 kg/m^3 [45] were used. Tests were carried out for two diameter ranges, i.e. 300–355 μm (mean diameter $\mu = 315$ μm and standard deviation in particle distribution $\sigma = 8.2$ μm) and 429–520 μm ($\mu = 475$ μm, $\sigma = 22$ μm). The velocity of the gas supplied through the side and main inlets was adjusted to reach 20 m/s at the supply channels. This was achieved by splaying 38.4 l/min and 240 l/min of air flow rates for side and main inlets, respectively. To check

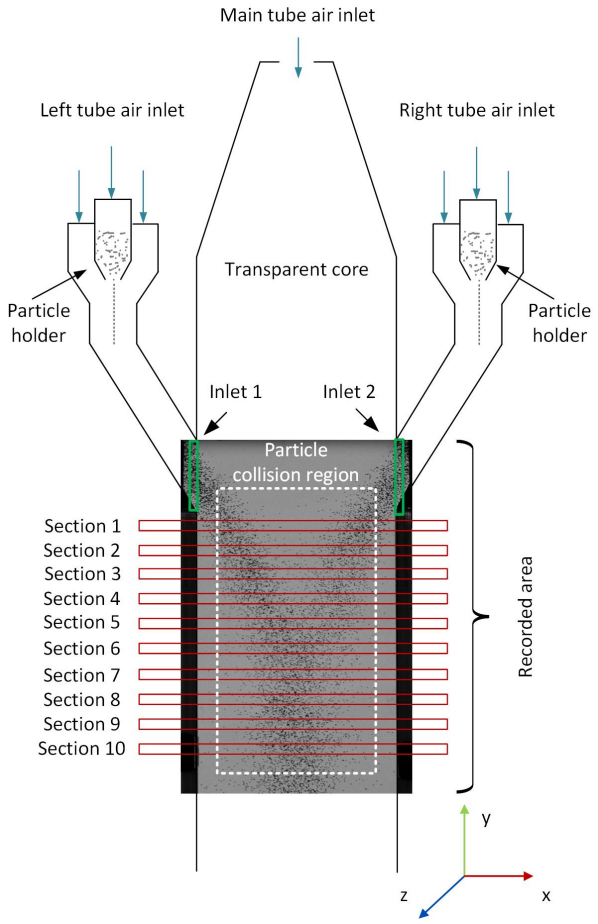

Figure 1: Schematic overview of the key elements of the test-rig and the part of the geometry captured by a camera together with marked locations, where data is extracted for model validation

the repeatability of the obtained experimental results, the measurements procedure, for given particles sizes and the test-rig configuration, was repeated nine times.

The time average mass flow rates of the particles determined, based on the analyzed particle flow rate in the inlet to the main channel, are marked in figure 1 as 1 and 2 for two considered particle ranges were 0.014/0.018 kg/s (left/right) and 0.013/0.019 kg/s (left/right) for particle mean diameter $\mu = 315$ μm and $\mu = 475$ μm, respectively. The total amount of used material, stored in the solid container before launching particles for both cases was 21 g, evenly divided between two particle holders.

To determine the accuracy of the numerical model, based on the experimental data, the measurement error need to be calculated. In practice, it is impossible to reach perfect consistency of the numerical and experimental results. In presented work, the law of error propagation [46] was used to determine the uncertainty of the experimental data. For two investigated particles ranges the uncertainties are related to the air regulators, time and space resolution of used camera. The uncertainty for particle mean diameter 315 μm was equal to 0.63 m/s, while for second one it was calculated at the level of 0.71 m/s. A detailed description of the procedure used for determination uncertainty for experimental results is given in [41].

3. Tested numerical models

The most popular approach used to model granular flow is the multifluid Euler-Euler (EE), which found a lot of practical applications [47, 48]. This model is very stable and all his features are well recognized and studied.

Nevertheless, the main bottleneck of EE technique is problem with modeling real particle size distribution (PSD) of the fluidization material. Most of applications uses two or three additional solid phase to represents PSD. Even in such configuration, the number of transport equation that need to be resolved can easily exceed 20. To resolve this problem, a Lagrangian technique was introduced [49, 50]. An example of the technique, which gives possibility to track particle in Lagrangian frame of reference, is the Lagrangian mulitiphase-particle in cell (MP-PIC) approach [49, 50]. For instance, only in ANSYS®Fluent software with semi-open structure, there are several available models, that can be used to model granular flows, for example the Hybrid Euler-Lagrange (HEL) [12, 15] approach that comes from MP-PIC and Discrete Element Method (DEM) [51]. In both of these approaches, the gas flow is modeled using the Eulerian approach, while the particles are tracked in the Lagrangian frame of reference. The main difference, between mentioned HEL and DEM approaches, can be noticed within used approach for modeling mutual interactions between particles. The HEL technique, collisions are modeled in the basis of the Kinetic Theory of Granular Flow (KTGF) [52, 53]. Collision between particles are determined in basis of the solid volume fraction in computational cell, where colliding particles are located. The second of mentioned approach for collisions forces calculation uses the common space position of to colliding particles and their velocity vectors [18].

Depending on selected approach the differences within predicted particle flow field can be expected. The advantage of the usage of the HEL approach is the calculation time, which is much shorter in contrary to DEM technique (for identical simulations the differences in times may be up to twenty). Nevertheless, the HEL approach required definition of the granular temperature Θ, standing for particle interactions, which can be evaluated using either transport equation or algebraic formula accepting some simplifications [54, 55, 20].

In application of the DEM the situation is quite different, as it was briefly mentioned. The DEM can use two sub-models for definition of the collision force that acts on the collating particles i.e., soft-sphere and hard-sphere [16]. For the detailed mathematical description of the DEM approach, the reader is referred to [56, 16, 57, 58].

For both approaches, the mass, momentum, energy, together with the turbulence need to be solved. The mass and momentum transport equations for the gaseous phase in instantaneous form are defined as [59]

$$\frac{\partial}{\partial t}\left(\varepsilon_f \rho_f\right) + \nabla \cdot \left(\varepsilon_f \rho_f \mathbf{u}_f\right) = S_{\text{mass}} \tag{1}$$

$$\frac{\partial}{\partial t}\left(\varepsilon_f \rho_f \mathbf{u}_f\right) + \nabla \cdot \left(\varepsilon_f \rho_f \mathbf{u}_f \mathbf{u}_f\right) = -\varepsilon_f \nabla p + \nabla \cdot \tau_f + \varepsilon_f \rho_f \mathbf{f} + K_{sf}\left(\mathbf{u}_s - \mathbf{u}_f\right) + S_{\text{mom}} \tag{2}$$

where the subscripts f denote the gaseous phases, ρ is the fluid density, $\mathbf{u}$ defines the velocity vector, and ε_g is the fraction of bulk phase. S_{mass}, S_{mom}, are the sources due to exchange of mass and momentum, respectively, between the continuous phases and particles. The momentum source term S_{mom} determines the change of momentum in the gaseous phase due to particle movement. K_{sf} is the average interphase drag coefficient. τ_f in is the stress tensor calculated for gaseous phase defined as

$$\tau_f = \varepsilon_f \mu_f \left(\nabla \mathbf{u}_f + \nabla \mathbf{u}_f^T\right) + \varepsilon_f \left(\lambda_f - \frac{2}{3}\mu_f\right) \nabla \cdot \mathbf{u}_f \bar{\mathbf{I}} \tag{3}$$

where λ_f is the bulk viscosity of the fluid phase, $\bar{\mathbf{I}}$ is the unit tensor, and μ_f represents the fluid dynamic viscosity. The particle motion equation, which equates the particle inertia with the forces acting on a particle is defined as

$$\frac{\mathrm{d}\mathbf{u}_p}{\mathrm{d}t} = F_{\text{D}}(\mathbf{u}_f - \mathbf{u}_p) + \frac{\mathbf{g}(\rho_p - \rho_f)}{\rho_p} - \frac{\nabla p}{\rho_p} - F_{\text{coll}} \tag{4}$$

where the subscript p refers to the particle data, ρ_p is the material density, $F_{\text{D}}(\mathbf{u}_f - \mathbf{u}_s)$ is the particle acceleration due to drag, term $-\nabla p/\rho_p$ defines the particle acceleration due to the pressure difference at the particle location, and F_{coll} defines the acceleration of the particle due to the collision's forces expressed as (4)

$$F_{\text{coll}} = \frac{\nabla \cdot \sigma_s}{\rho_p} \tag{5}$$

where collision tensor σ_s is defined as

$$\sigma_s = -p_s \bar{\mathbf{I}} \tag{6}$$

and granular pressure p_s which defines the interactions between particles can be calculated as [60]

$$p_s = \underbrace{\varepsilon_s \rho_s \Theta}_{p_{s,\text{kin}}} + \underbrace{2\varepsilon_s^2 \rho_s (1+e_{ss}) g_{0,ss} \Theta}_{p_{s,\text{col}}} \tag{7}$$

where ε_s stands for the solid volume fraction, e_{ss} defines the restitution coefficients while $g_{0,ss}$ expressed the radial distribution function. The granular temperature Θ in discussed work was calculated using the algebraic formula [61]

$$-\nabla p_s + \tau_s : \nabla \mathbf{u}_s - \frac{12(1-e_{ss}^2) g_{0,ss}}{d_p \sqrt{\pi}} \rho_p \Theta^{3/2} \varepsilon_s^2 - 3K_{sg}\Theta = 0 \tag{8}$$

where the third and forth terms in above equation stands for energy dissipation and the energy exchange between phases, respectively. A graphical representation of a collision model used in the DEM technique is shown in figure 2. Used model gives possibility to take into account the deformation of the particles due to their contact indicated by the particle overlapping δ parameter. The acceleration of the particle due to the collisions in DEM technique is expressed as

$$F_{\text{coll}} = \mathbf{F}_1 = -\mathbf{F}_2 = K_H \delta^{3/2} \mathbf{e}_{12} \tag{9}$$

where K_H is the physical material property, determined from the respective Young's Moduli E_1 and E_2 of the two colliding particles and their Poisson's ratios ν_1 and ν_2

$$\mathbf{K_H} = \frac{4}{3} \frac{E_1 E_2}{E_2(1-\nu_1^2) E_1 (1-\nu_2^2)} \sqrt{\frac{r_1 r_2}{r_1 + r_2}} \tag{10}$$

the unit vector from particle 1 to particle 2, is calculated using a simple expression

$$\bar{\mathbf{e}}_{12} = \frac{\mathbf{x}_2 - \mathbf{x}_1}{||\mathbf{x}_2 - \mathbf{x}_1||} \tag{11}$$

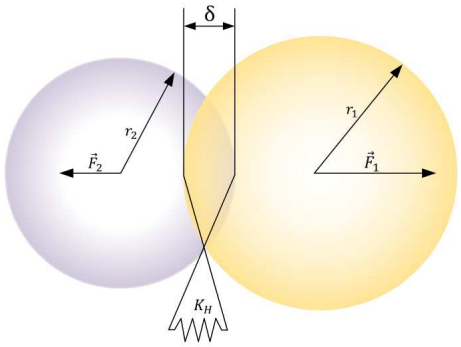

Figure 2: Exaggerated collision effect between two particles

A crucial aspect when modeling granular flow with application of DEM, is the use of an appropriate time step. To determine the exact time step, the methodology described in [62] was used. It is determined on the basis of determining three different time steps based on the physical properties of the material being used, Raleigh, Hertz, and Cundall. The simulation time step is selected from the relation

$$t = 0.2 \cdot \min\left(t_{\text{Raleigh}}, t_{\text{Hertz}}, t_{\text{Cundall}}\right) \tag{12}$$

The Raleigh and Hertz time formulae are determined and briefly described in LIGGGHTS documentation [63]

$$t_{\text{Raleigh}} = \frac{\pi r_{sphere}}{0.1631(\nu + 0.8766)} \sqrt{\frac{\rho_p}{E/[2(1+\nu)]}} \tag{13}$$

while the Hertz time step is defined as

$$t_{\text{Hertz}} = 2.87 \left[\frac{(\rho_p (4/3)\pi {r_{sphere}}^3)^2}{r_{sphere} E^2 V_{max}} \right]^{0.2} \tag{14}$$

The Cundall model used in the software LS-DYNA DEM [64] for definition time step is

$$t_{\text{Cundall}} = \sqrt{\frac{\rho_p (4/3)\pi {r_{sphere}}^2)}{\frac{E}{[3(1+\nu)]} NORMK}} \tag{15}$$

where $NORMK$ is a stiffness penalty parameter, typically ranging between 0.1 and 0.001. For this particular case, the penalty parameter was chosen to be equal to 0.001. The time step used in the presented study, for the considered material was $2.46 \cdot 10^{-7}$ seconds.

4. Novel collision approach

There are some disadvantages of both models, listed in the previous section. The precision of the HEL approach, depends on the calculated value of the granular temperature, which can also cause some stability problems. Undisputed advantages of the HEL technique are the calculation time and the possibility of direct incorporation of real PSD to represent the fludization process. The DEM approach is accurate, but it is time-consuming, and is applicable rather for small-scale cases. To take advantage of both approaches, that are calculation time and collision accuracy, a hybrid collision model developed in the framework of machine learning (ML) is proposed here. The purpose of the surrogate model (SM) developed based on machine learning (ML) is to replace the standard KTGF approach used to model the term F_{coll} in equation (4) of the HEL technique, creating the HELSCM approach. The built surrogate model allows one to eliminate the problems that are behind the calculation of the granular temperature Θ, and at the same time, increases the stability of the solution process. At the same time, by using the HELSCM technique, the calculation time required to model the granular flow, can be reduced while maintaining the accuracy required in collision prediction.

Literature study and gain experience in various ML applications, influenced to choose the XGBoost (Extreme Gradient Boosting) algorithm [65] to create the reduced order model. XGBoost is based on supervised machine learning [66], decision trees [67] and gradient enhancement [68]. The predictive model is designed to solve regression problems [69, 70, 71], based on the supervised learning method. In this approach, the model is created by decision trees by evaluating a tree asking conditional questions (if/then/else) [72] and deciding if an option is true or false. The minimum number of questions must assess the probability of making a correct decision. In such a way, the algorithms learn the relationships between features (input data) and the target (output data). A brief description of XGBoost can be found in [73].

4.1. Data set generation procedure

Before the generation of the supervised ML model, the required data set must be collected for the considered task. To develop a surrogate collision model, the input and output parameter configuration need to be a priori known. Here, as shown in figure 3 the input and output data correspond to the velocity vector components of two colliding solid particles. Moreover, developed data stores also information about particle size and density in case of future ML model extension, e.g. application for the polydisperse cases, while presented work is focused only on monodisperse system. As mentioned earlier, the low-scale DEM model was used to generate the required data. In this case, the Cundall and Stack [74] approach was used to model particle interaction implemented in ANSYS®Fluent was used. Selected configuration of the low-level DEM collision model is the simplest, least

complicated approach, and does not expose the developer to error, when modifying the behavior of the particles in the system.

The data set generation process is initialized by determining the velocity range (V_{mag}) for the colliding particles. On the basis of experimental data, the velocity magnitude range was set from 0 m/s to 20 m/s. The set of equations used for the calculation of the components of the velocity vector for the defined angles φ and θ based on the velocity magnitude of the particle is defined as

$$\begin{aligned} u_{A,B} &= V_{\text{mag}} \cdot \sin\theta \cdot \cos\varphi \\ v_{A,B} &= V_{\text{mag}} \cdot \sin\theta \cdot \sin\varphi \\ w_{A,B} &= V_{\text{mag}} \cdot \cos\theta \end{aligned} \tag{16}$$

where φ is the angle defined from the OX axis, and θ is the angle defined from the OZ axis as illustrated in figure 4(A). Figure 4(B) presents the distribution of particle velocity configurations after determining the components of the particle velocity vectors. For clarity, the particle velocity vectors are not marked here, while each direction is pointed to the center of the coordinate system.

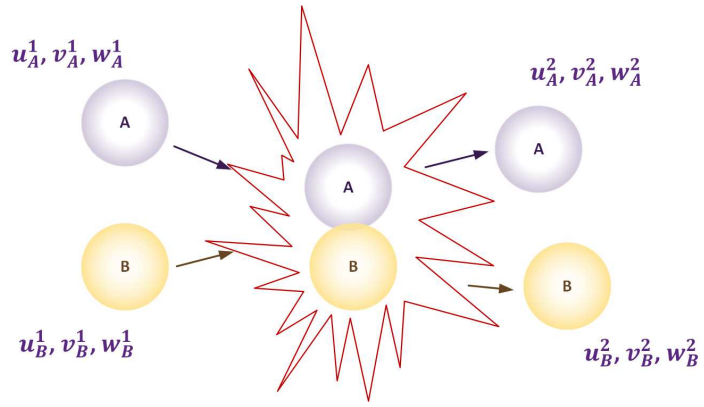

Figure 3: Configuration of the low-level collision model used for collecting data set for ML model

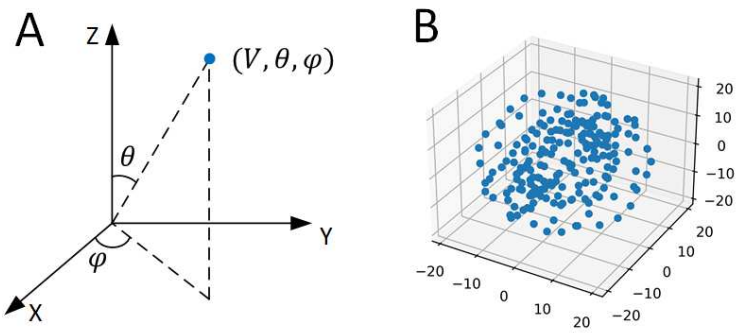

Figure 4: **A:** Visualization of the methodology used for the calculation of the velocity components based on spatial particle location and its velocity magnitude, **B:** distribution of the points that corresponds to particle position according the velocity vector configurations pointed into the center of coordinate system

To collect the data set by applying the low-dimensional collision model, the spatial configuration of two colliding particles need to be accurately defined. In the model used, the velocity vectors and position of two particles were configured in such a way, to ensure that both particle will collide in the center of coordinate system. It is an important point because introducing data into the model about particles that did not collide with

each other, would not only decrease the performance of the model but would also increase the number of possible configurations, and thus increase the computation time of the data set generation stage. All of the mentioned operations are also required to prevent a situation, where two colliding particles in a certain time step overlap. Such a situation will cause a disproportionately large deformation of the particles, and this would directly affect the velocity after the collision; it would be very high (about 100 m/s - although such velocity depends on the model constraints, in this case the defaults were used), which would not correspond to the reality.

Apart from the need to determine the turns of the velocity vectors of the particles to the center of the coordinate system, it was necessary to also take into account other possible collision configurations between the particles. The possibilities of particles colliding with each other are illustrated in figure 5. Figure shows only a view of possible particle behaviors, where their post-collision reaction may be exaggerated. Particles can collide with each other with the same velocity vector turns as depicted in figure 5 (A) but, with different configurations of the assumed velocity values. Another possibility is the so-called parallel collisions, highlighted in figure 5 (B), where the particles move in the same direction, but the particle at the back has a higher velocity, so that after the collision, a part of the force is transferred to the particle moving in the front, which increases its velocity. Another possible configuration is the head-on collision, where the velocity vectors of the particles are opposite, as shown in figure 5 (C).

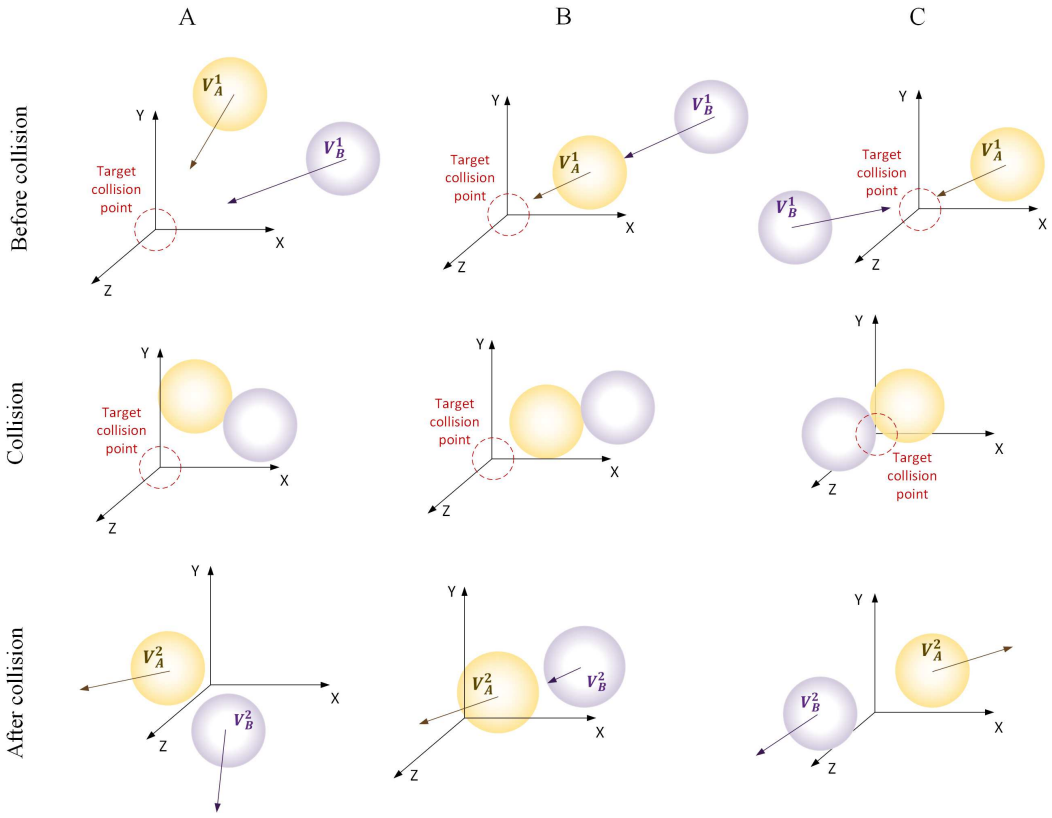

Figure 5: Approximate visualization of possible collision configurations and the stage before, at and after the collision. Column A shows a possible collision of particles moving in the same direction, column B of particles moving in so-called parallel and column C of head-on collisions

The data generation and simulation process was fully automated. It was possible through a combination of Python scripts and Ansys® Fluent software. Once the control code was created, the particle positions and velocities (based on the above formulas and assumptions) for 60 000 collision configurations were determined. Following the flow chart shown in figure 6, the process started from reading the file with all configurations. Then, from the first 100 combinations, 200 injection files (two for each simulation) were created. Then, a journal file

was created that, without restarting the program, loaded the corresponding cases and the corresponding injection files. This approach was necessary to reduce the computation time by reducing the number of Ansys® Fluent opening from so-called zero. However, at the same time, maintaining the security of not losing data from all the cases already recalculated. Such security, in the case of random situations such as power cut or license problems, means that at most 100 simulations had to be repeated, rather than all of them starting from the first. At the end of each simulation, using a specially developed user-defined function (UDF), the components of the velocity vectors of each particle were saved in a file. In addition, with such a large amount of data, great care must be taken not to mix up the data, that is, each input must correspond to a specific output. Therefore, each case was labeled with a specific number. Another applied calculation speed-up trick, was the division of the main file into 10 smaller ones, so that calculations could be carried out simultaneously in separate programs. The whole procedure described above was carried out without any changes. After many attempts, by synchronizing the calculations, reducing the number of program openings, and not losing large amounts of calculated data due to random events, the total data generation time was reduced to about a week.

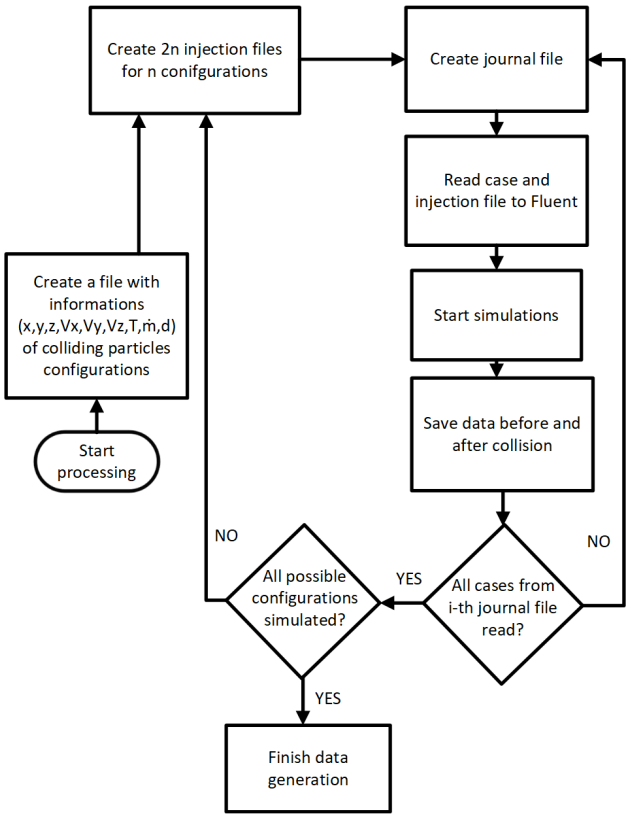

Figure 6: Flow chart presenting automation of the data generation process

4.2. Development ROM model generation

Each time, before building the model itself, the data set should be divided into three subsets: test, training, and validation. The first one is not included in the process of training the model, but in the final stage for that one metrics are set, which determine whether the model is satisfactory enough. It is discussed here that the test data set represents 5% of the total data. After the test set was separated, the data were divided into 75% for the training set and 25% for a validation set. The next step in data preprocessing is the application of the standardization technique [75]. To reach a stable solution and high precision in predicting target parameters, the data was standardized, that is, rescaled relative to their mean and standard deviation, according to formula [76]

$$\mathbf{X}_{sc} = \frac{\mathbf{X} - \mu_{train}}{\sigma_{train}} \tag{17}$$

where $\mathbf{X}_{sc}$ is the standardized value, $\mathbf{X}$ is the original value, μ_{train} and σ_{train}, respectively, denote the mean and standard deviation determined for the training set. Then, using the calculated μ_{train} and σ_{train}, the test and validation sets were standardized.

When building any surrogate model in frame of the ML, it is important to define the hyperparameters that affect its performance [77], that is, the quality of the prediction results. Hyperparameters can be selected using dedicated libraries, allowing us to choose them in the most efficient and effective way. Such libraries offer optimization tools that allow, in a relatively short time, to obtain the best hyperparameters, allowing to obtain accurate models. Of several available tools, Optuna [78] was chosen to find the best values. Optuna formulates hyperparameter optimization as a process of minimizing/maximizing an objective function, taking a set of hyperparameters as input and returning with its (validation) score. During the process, the search space is narrowed using records of suggested parameter values and evaluated objective values, leading to an optimal search space that consists of parameters that lead to better objective values. During the search for hyperparameters, pruning is also used, which is responsible for interrupting calculations when there is no improvement in accuracy. Such an approach reduces the cost of computation, further reducing the search time.

The hyperparameters that were chosen to optimize, were three, the basic and most frequently modified to improve model quality, i.e.

- n_estimator — number of gradient boosted trees, equivalent to the number of boosting rounds,
- max_depth — maximum tree depth for base learners,
- learning_rate — boosting learning rate,
- colsample_bytree — defines what percentage of features is used for building each tree,
- reg_alpha — L1 regularization term on weights.

It was decided to perform 50 trials using Optuna [78] procedure to find the best hyperparameters. Each time, five of the hyperparameters mentioned above were changed and used to build a model on the train data set. After building a model, using a validation set, the accuracy of the model was calculated. After conducting 50 procedure evaluations, the one that gave the highest precision was selected for future processing, saving the corresponding hyperparameters [65].

The main task of the novel collision model is to predict, based on‘ the components of the velocity vectors of two colliding particles, the components of the velocity vectors for the particle involved in the collision after it occurred. There were two different approaches that could be considered when building the models. The first was to build a single model that predicts the three components of the velocity vectors in a single step. This solution, only at first sight, is a good one. Unfortunately, when the models were built in this way, they were not sufficiently accurate. It is essential that the mean absolute error (MAE) be as small as possible because, at low velocities, with which we are dealing, even a small error, deviating from the expected value has a great influence on changing the trajectory of the particles. Therefore, an approach that is often practiced, i.e., the construction of three separate models, where each model predicts only one velocity component. In this way, it was possible to reduce the error made in the prediction of individual values, which is essential in this particular case, while not affecting the timing of the model calling during the solution procedure. The final MAEs for the subsequent models used for both investigated particle sizes were equal to $\mathrm{MAE}_{u,v,w}$ =(0.5877;0.5802;0.5531) for $\mu = 315$ μm and $\mathrm{MAE}_{u,v,w}$ =(0.7078;0.7276;0.6078) for $\mu = 475$ μm.

The metrics for the trained models that cover both investigated particle diameters for the test sets are shown in the graphs 7, where the predicted and exact values are shown for the *test data set*. Ideally, the plotted points should perfectly coincide with the diagonal on the marked graph. For each of the three models for subsequent velocity components, the predicted values are close to the real data. There are only single values that deviate significantly from the expected values. The bar graph 8 shows that most of the tested configurations return the predicted velocity with an error lower than 5%.

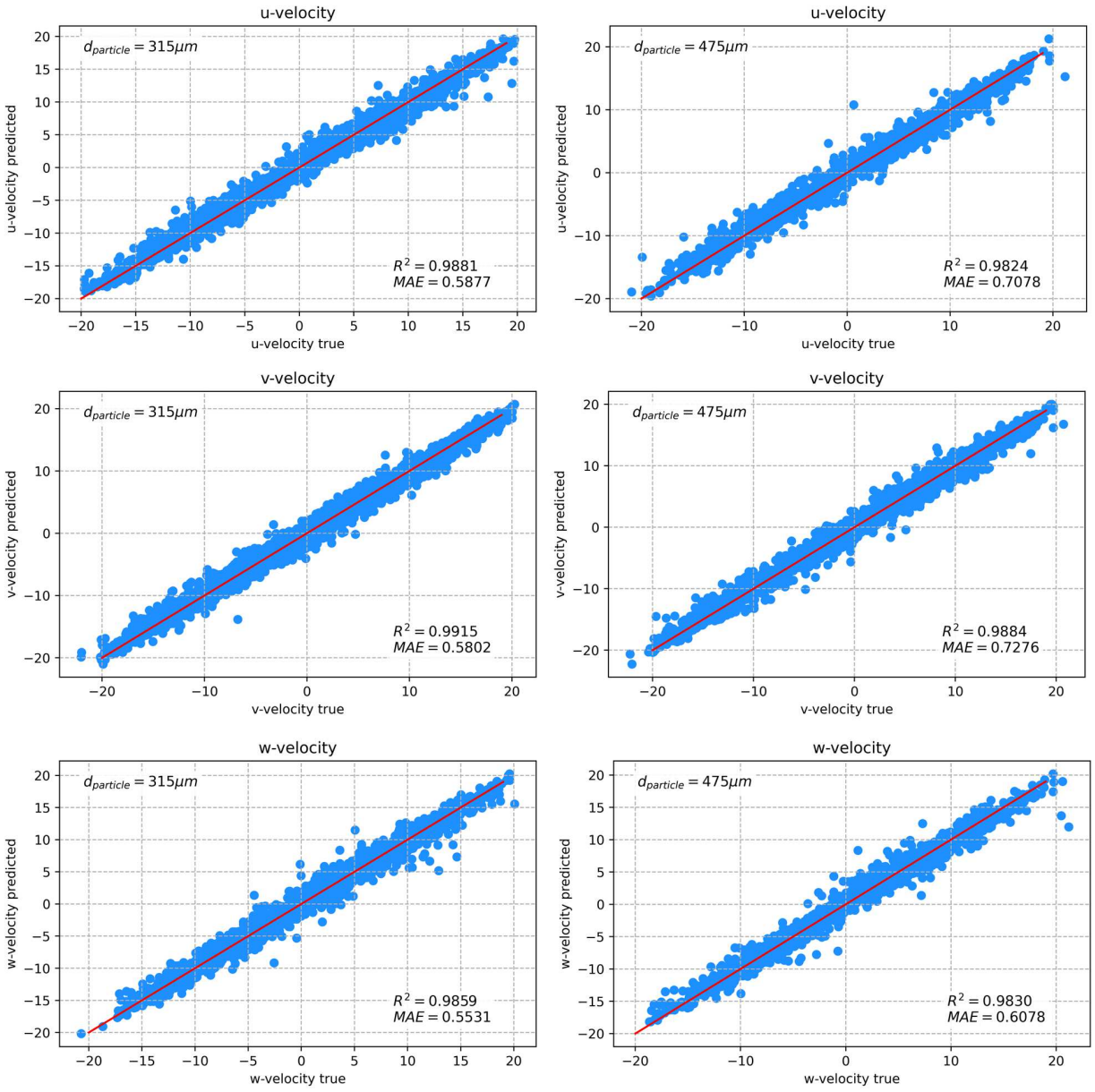

Figure 7: Comparison of predicted and true values for each of the velocity components for models built for different velocity components using the *test data set*. The red line indicates the diagonal around which the predictions with true values should be placed. In addition, the accuracy values (MEA) for the test sets are marked.

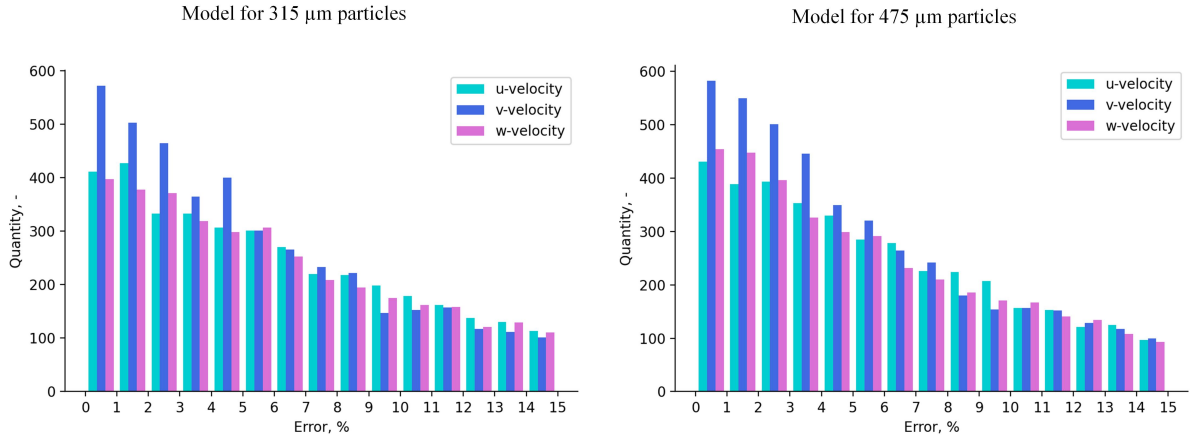

Figure 8: Distribution of the calculated relative error between exact and predicted velocities for both investigated particle sizes, i.e. $\mu = 315$ μm (left) and $\mu = 475$ μm (right)

4.3. Surrogate collision model implementation

Once the surrogate model was developed, it was required to implement it into the CFD code. Presented studies uses the ANSYS®Fluent CFD code, while the model can be freely implemented into an open source CFD code. Implementation of a developed collision model into the HEL approach, to create HELSCM, requires model adaption for used CFD software. The general overview of the implementation can be seen in figure 9. In the collision model implementation, the collision is detected in a way similar to that, used in the DEM to have the chance to compare both models. At the end of each time step, the position and velocity components of the colliding particle are found. If the distance between the center of the particles was smaller than the sum of their radii ($|P_A P_B| < r_A + r_B$), a collision was detected and the velocity components of the colliding particles were saved. In each subsequent collision, the velocities of subsequent colliding particles are added, note that the velocities are saved for both particles involved in the collision. At the end of the collision detection loop, for each cluster of colliding particles, the average velocity components were calculated. After the determination of the average velocities (for pairs of colliding particles), the surrogate regression model returns the values of the velocity components, after the collision as illustrated in figure 9.

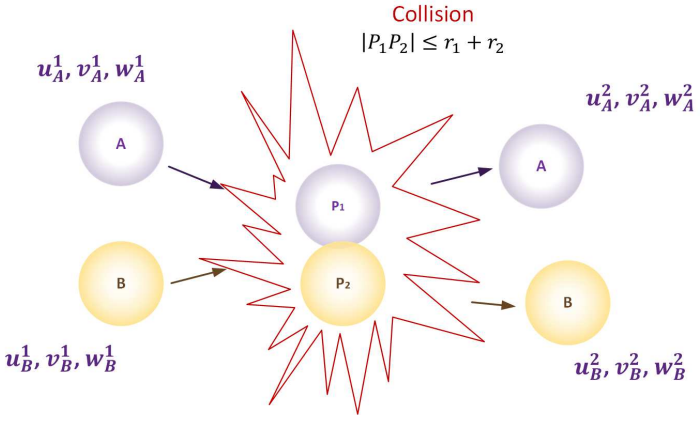

Figure 9: Implementation of the reduced-order model developed in the CFD code, where P_1 and P_2 respectively particle centers, r_1 and r_2 the particle radii, and u, v, w are the velocity vector components for particles A and B, before and after collision

5. Geometrical model of the test-rig

To perform numerical simulations, the unambiguity conditions, i.e. geometry, boundary conditions, initial state, and material properties, must be known *a-priori*. The computational domain was built on the basis of the 3D model of the test rig with verification in reality. In order not to provide many complications into the model, and to be able to reach numerical results in reasonable time span, the original geometry was simplified, mostly to eliminate complicated geometry elements. For example, to model particle injection, the idea of volume injection was used, instead of using complicated geometry of the particle holder (see Fig. 1). This particle injection strategy, requires the definition of the particle mass and the number of tracked parcels. The mass is known from the experiment, while the parcel number is calculated in order to ensure each parcel storing only single particles to represent reality. Moreover, the initial particle velocity of the injected particle needs to be defined. As mentioned above, part of the air delivered to the rig, was pushed through the particle holder; some initial velocity of the particle can be expected. To check this, additional simulation was carried out using the DEM approach and complex particle holder geometry, to check the particle velocity at the outlet from the particle holder. Simulations showed that the magnitude of particle velocity can reach 3.4 m/s at that location.

To perform simulations, the computational domain was discretized using only hexagonal elements with a skewness coefficient of less than 0.22 (mean: $4.092{\cdot}10^{-2}$), where the mesh resolution was 107,000 elements. Such grid was chosen based on the mesh sensitivity analysis already presented in [79]. To solve a set of transport equations, that is, the mass, momentum and turbulent transport equations, the phase-coupled SIMPLE solver [48] was used in the calculations. For the momentum equation, a second-order discretisation scheme was selected. For the continuity equation, the QUICK scheme [80] and for time discretization, the first-order implicit scheme was used.

To quantitatively compare the set of numerical results, ten mentioned sections downstream of the inlets along the main channel, where particle velocities were determined, were specified. The investigated locations of the profiles, in the numerical model, are visualized in figure 10. Furthermore, the dimensions are marked, so that the exact position of the sections can be determined. For each case considered, the velocity profiles of particles in motioned locations, averaged over time, are used to investigate the differences between models.

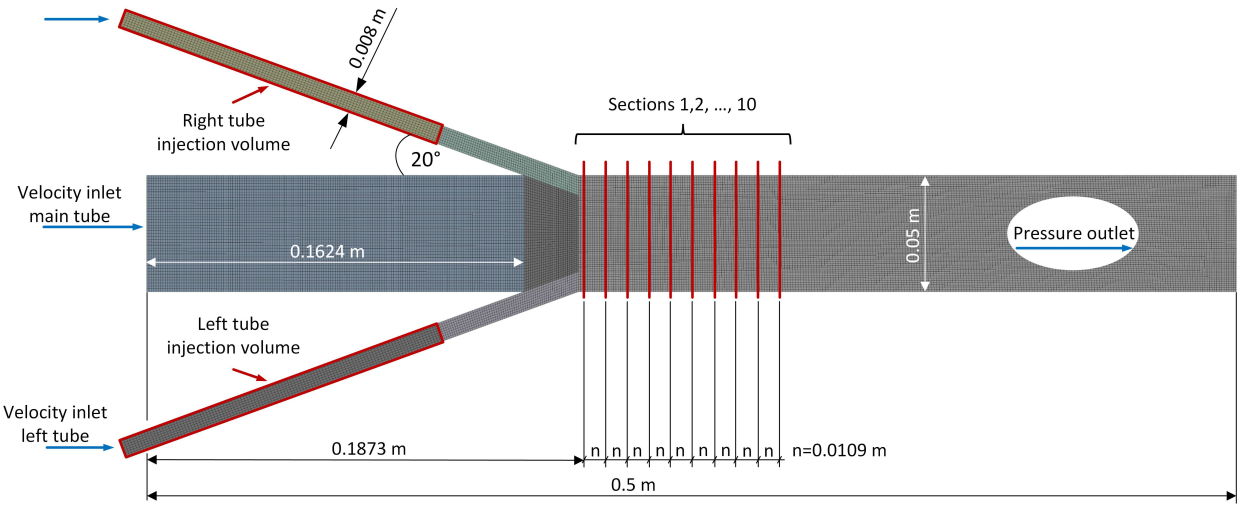

Figure 10: Geometry, with marked boundary conditions and locations of ten sections, where the average particle velocities profiles were determined and used for model validation

6. DEM and HEL models comparison - initial results

One of the first steps was the comparison of standard HEL and DEM approaches using the particle with mean size 315 μm. To compare both models, numerical simulations were carried out for three different time steps, i.e.

$\Delta t = 10^{-3}$ s, 10^{-4} s and $7.14 \cdot 10^{-5}$ s. The first time step size is typical to be used in the case of application of the HEL approach [12], while the last time step size is the resolution of the frames, recorded during experimental work [41]. The purpose of these simulations was to check the impact of the time step on collision detection by both models. Furthermore, using the HEL model, two configurations were investigated. First, where the number of particles in the parcel was equal to the unit corresponding to the particle mass equal to 0.000196 kg (12,000 particles) and second, where the mass of injected particles was increased to 0.0018 kg. In the second case, the number of particles in the parcel increased to 8, simultaneously affecting the solid volume fraction. To model the collision by application of the HEL approach, using the KTGF set of closure terms that need to be modeled. The list of used submodels is presented in Table 1.

Table 1: Closure models and parameters used in the simulations, where model names are given as they appear in ANSYS®Fluent CFD code

Solid pressure, p_s	lun-et-al [60]
Radial distribution, $g_{0,ss}$	lun-et-al [81]
Granular viscosity, μ_s	gidaspow [20]
Granular bulk viscosity, λ_s	lun-et-al [60]
Frictional viscosity, μ_{fric}	schaeffer [82]
Frictional pressure, p_{fric}	based-ktgf [61]
Granular temperature, Θ	algebraic [61]
Drag model, K_{sg}	gidaspow [20]
Restitution coeff. in solid phase, e_{ss}	0.9
Friction packing limit, $\varepsilon_s^{\text{fric}}$	0.61
Packing limit, $\varepsilon_s^{\text{pk}}$	0.63
Transition factor of HEL	1.0
Particle–wall reflection coeff.	$e_{nor.}$=0.8; $e_{tan.}$=0.8

The main difference, between the DEM and HEL approaches, is the way in which collisions between particles are taken into account. Figure 11 (top), shows the distribution of particles obtained after 0.03 s of numerical simulation, while figure 11 (bottom) shows the contours of the solid volume fraction. The DEM shows a qualitatively better collision effect of two colliding particle streams, contrary to the HEL approach. In the latter approach, collisions are detected based on the solid volume fraction in the computational cell and based on the calculated value of the granular temperature [83]. Even with increasing solid volume fraction, it can seem that the collision rate in the HEL approach was not improved. The decreasing time step used for the numerical simulation, which should naturally affect the number of possible collisions detected by the HEL approach, was not observed. The interactions of particles from opposite streams are negligible when using the HEL approach, as can be observed in figure 11. The particles streams interpenetrate each other, as indicated by the lack of change in the trajectory of the moving particles. From the application perspective, the determination of the direction of particle movement after collision, their trajectories, simulation time, and accuracy are very important in the case of reproducing reality by a numerical model.

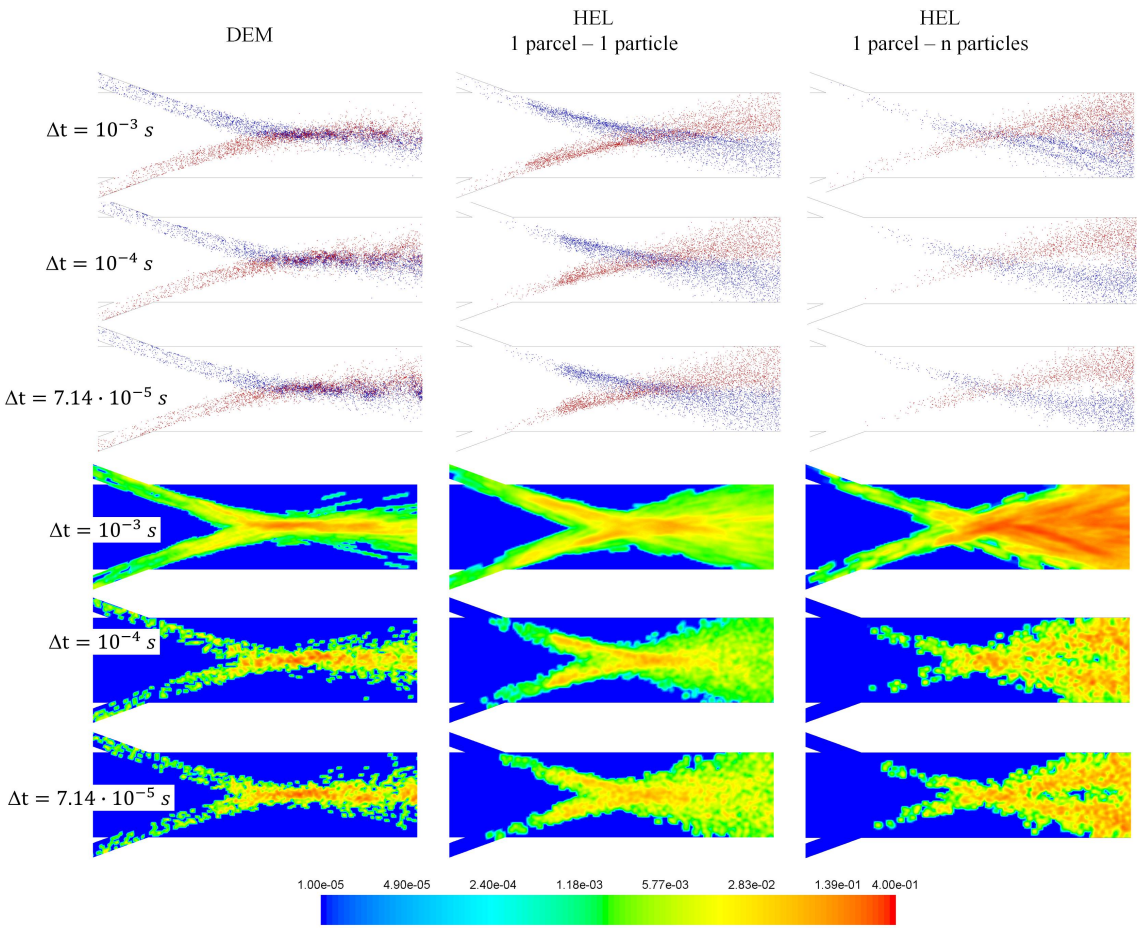

Figure 11: Qualitative comparison of the hybrid Euler-Lagrange (HEL) and discrete element model (DEM), applied to the modeling of two streams of colliding particles. The upper part shows the particle distribution (blue colored-right stream, red colored-left stream), and the lower row illustrates contours of the solid volume fraction (presented in logarithmic scale) after 0.03 seconds of numerical simulation. 1 parcel containing 1 particle (tracked parcel consists of only a single particle), while n particles mean that the number of parcels was kept constant, while the number of particles in the parcel increased with increasing mass of the injected material.

Figure 12 shows the differences in the calculation times of the wall clock between the models used. It is clear that the DEM technique is much slower, in contrast to the standard HEL approach. In the model configuration discussed, only thousands of particles were tracked, which also causes a long execution time. Application of DEM for industrial scale, despite high computational effort, the wall clock time would stretch into months or years. As the time step Δt decreases, the frequency of collision detection increases. It makes the determination of the collision forces, resulting from each collision, very computationally and time-consuming, as can be clearly noticed in the comparison of simulation times shown in figure 12. The HEL approach gives the possibility of a significant reduction in the computation time, but, consequently, a collision effect is attenuated, as shown in figure 11. The HEL approach is also very sensitive to the numerical resolution of the mesh, which mainly affects the calculated drag force that acts on the solid clusters [84] and the volume fraction of the solid. The implementation of the HEL approach, for drag calculation in motion equation, uses the diameter of the parcel instead of the diameter of the particles, which also affects the sensitivity of the HEL approach.

Taking into account the significant differences in the accuracy in detection particle collision and simulation time, it is straightforward that the model which will combine the advantages of both mentioned computational techniques is highly demanded especially for industrial, large-scale applications where the balance between accuracy and computational cost needs to be preserved.

The new collision model developed in this work will be implemented into the solution procedure of the

standard HEL model to replace the KTGF collision model, which combines the accuracy of the DEM in prediction of the mutual particle interactions, while at the same time the computation wall-clock time is of two-three orders faster in contrary to the standard DEM approach.

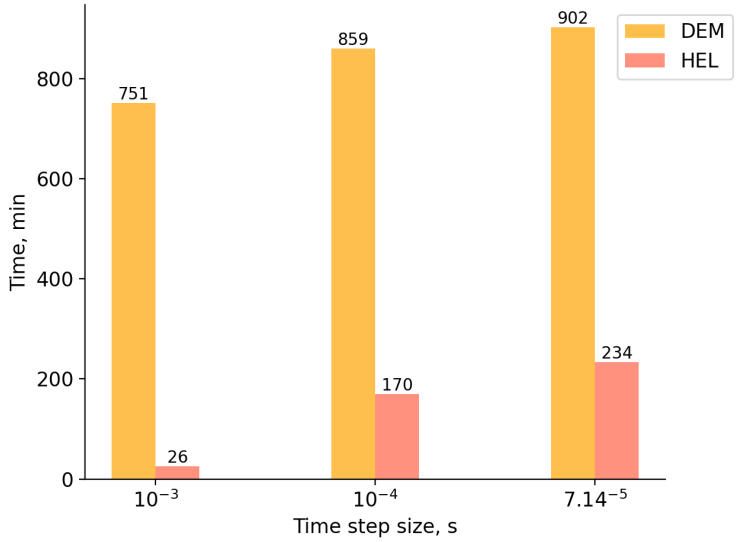

Figure 12: Comparison of HEL and DEM simulation time

7. Testing functionality of HELSCM technique

Before applying the collision model developed for exact CFD simulations, a simple set of tests was carried out. Performed tests consist only of the two groups of colliding particles. The physical properties of the particles corresponded to those used in the experimental work. The main focus was on comparing the behavior of the particles in a situation where their share of solid volume in the computational cell is small. Figure **??** shows the results using the following three models: HEL, DEM, and in this work developed the HELSCM approach. For each of the scenarios, three moments of the collision were investigated, that is, before, at and after. The cases that were taken for verification represent two streams of three particles moving against each other with an angle of 20 degrees at a speed of 5 m/s. Particles were introduced into the domain in the first three time steps. The size of the time step was equal to 10^{-4} s.

The initial position of the injected particles was determined so that they would definitely collide after the fifth time step. Thus, the behavior of the particles during this process can be clearly observed. In the case of the HEL model, the particles overlap at the moment of collision; there is no collision effect in the form of expected reflection, which results in two streams passing each other. At that moment, a collision between the red and blue particle streams occurred. It is worth mentioning here that the volume fraction based on which the granular temperature in KTGF is used is smaller than 0.06, which directly affects the results showing a lack of collision between tracked particles. In the case of usage of the DEM model, the particles immediately bounce off and change their direction of motion to the opposite, while the collision was detected which can be seen looking at the blue and read particles. Using the HELSCM (surrogate collision model), the particles as in the HEL approach overlap at a given time step. However, when collisions are detected, when the distances of the particle centers from each other are smaller than the sum of their radii as shown in figure 9, the surrogate model is called. The model returns the corresponding components of the velocity vectors. Thus, particles with this collision configuration change their trajectory to the opposite, similarly as in the DEM technique.

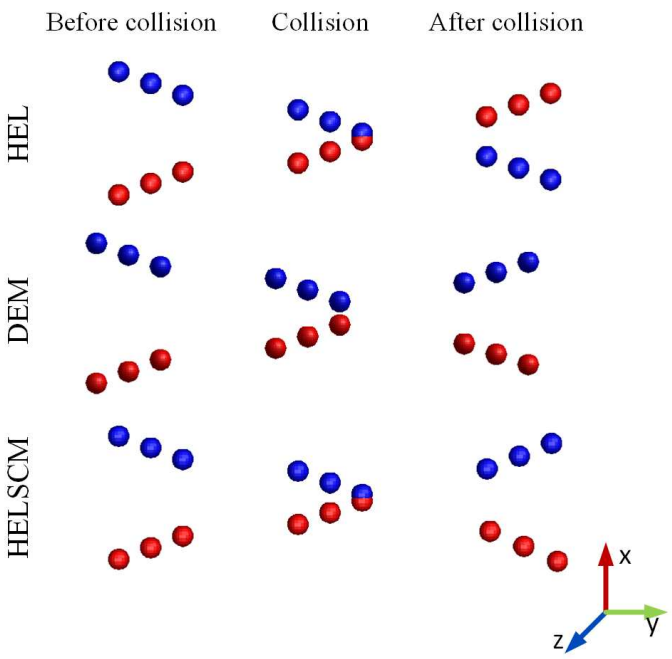

Figure 13: Testing proposed HELSCM technique for modeling granular flow by its comparison to the standard HEL approach and the DEM, in small scale to capture of models features where each model functionality is presented based on particle stream behavior before, at and after collision

8. Lab-scale application of HELSCM collision model

The purpose of this part is to compare qualitatively and quantitatively the results obtained by applying the HELSCM technique with the experimental data and results obtained from the DEM model. For modeling the mutual interaction of two colliding particle streams, the computational geometry shown in figure 10 was used. The set of simulations was carried out for three simulation time steps, i.e. $\Delta t = 10^{-3}$ s, 10^{-4} s and $7.14 \cdot 10^{-5}$ s. Numerical simulations were performed for two mean particles seizes, i.e. 315 μm and 475 μm. The particles were placed in the computational domain using a volume injection strategy (see Fig. 10 with marked injection volumes). The particle mass was equal to 0.000196 kg and the number of particles was equal to 12,000 particles and 3600 for 315 μm and 475 μm, respectively. For both investigated particle sizes, the overall particle mass was evenly distributed between two particle holders. The number of particles injected for case 475 μm was reduced to not overtake the limited injection volume. In this way, the number of particles in the parcel for both investigated cases was kept unit. According to that, the initial solid volume fraction was kept the same for both investigated cases.

To discuss the HELSCM approach, more attention was paid to the results obtained using particles with a mean diameter equal to 315 μm. The first step of the model testing was to check how the division of the boxes used for calculation velocity profiles affects them. Three-box resolution was tested, that is, 20, 88, and 126 of subboxes as can be seen in [41]. Figures 14, 15, and 16 illustrate the comparison of the calculated time-average solid velocity profiles using the HLESCM and DEM approaches, compared to the experimental data. By increasing the box resolution, a better representation of the particle velocity was achieved, mainly in three front locations where the particle death zone occurs, in the vicinity of the particle injection channels. This is caused by decreasing the number of particles in subsequent sub-boxes that are used for averaging. However, for 88 and 126 of the subboxes no significant differences between evaluated solid velocity profiles were observed.

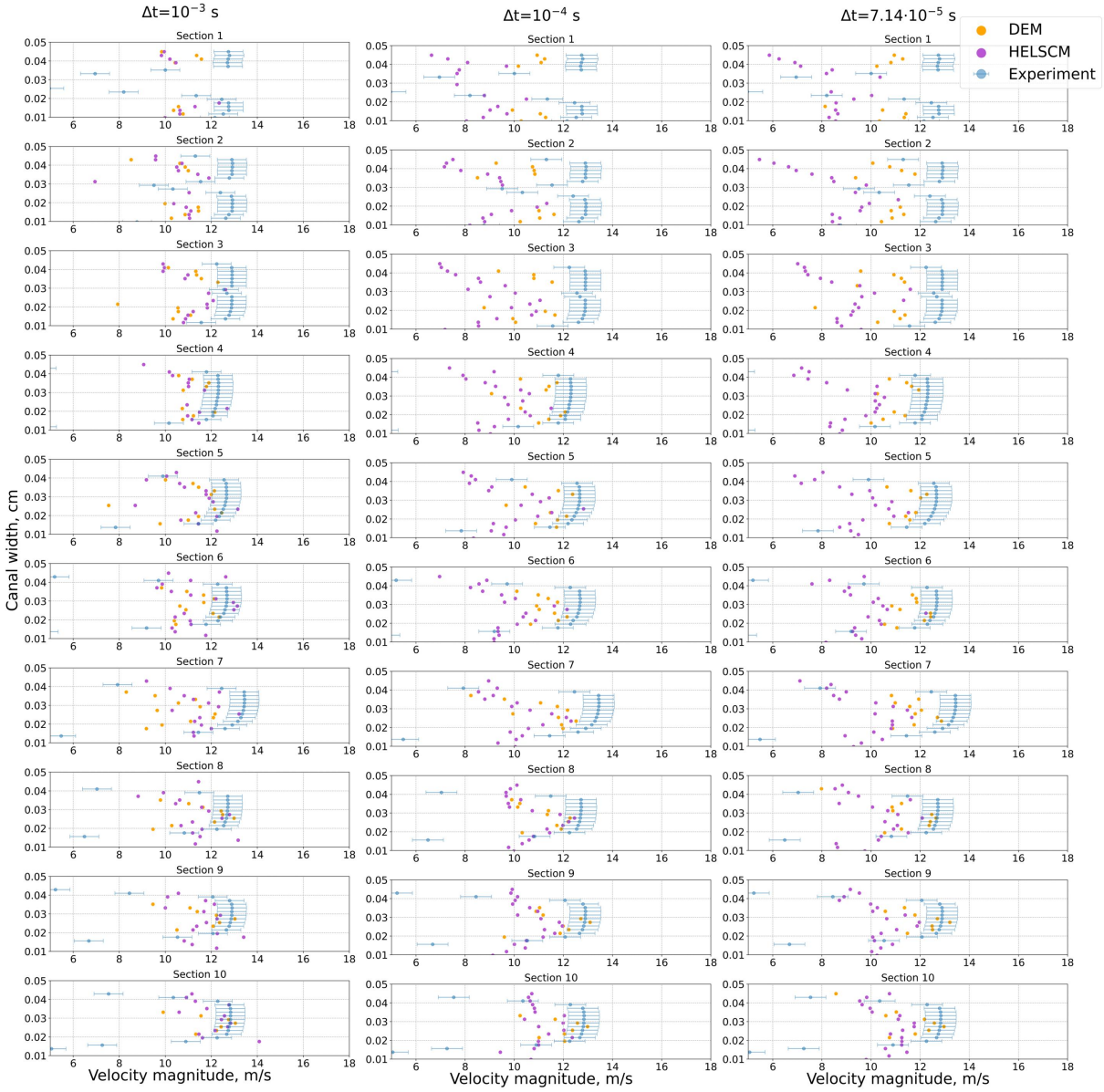

Figure 14: Quantitative comparison of the DEM and HELSCM model based on calculated particle velocity profiles, at ten location downstream of the computational domain (see Fig. 10), obtained for different time steps for particle size 315 μm after 0.02 seconds of numerical simulation and using 20 boxes for profiles reconstruction

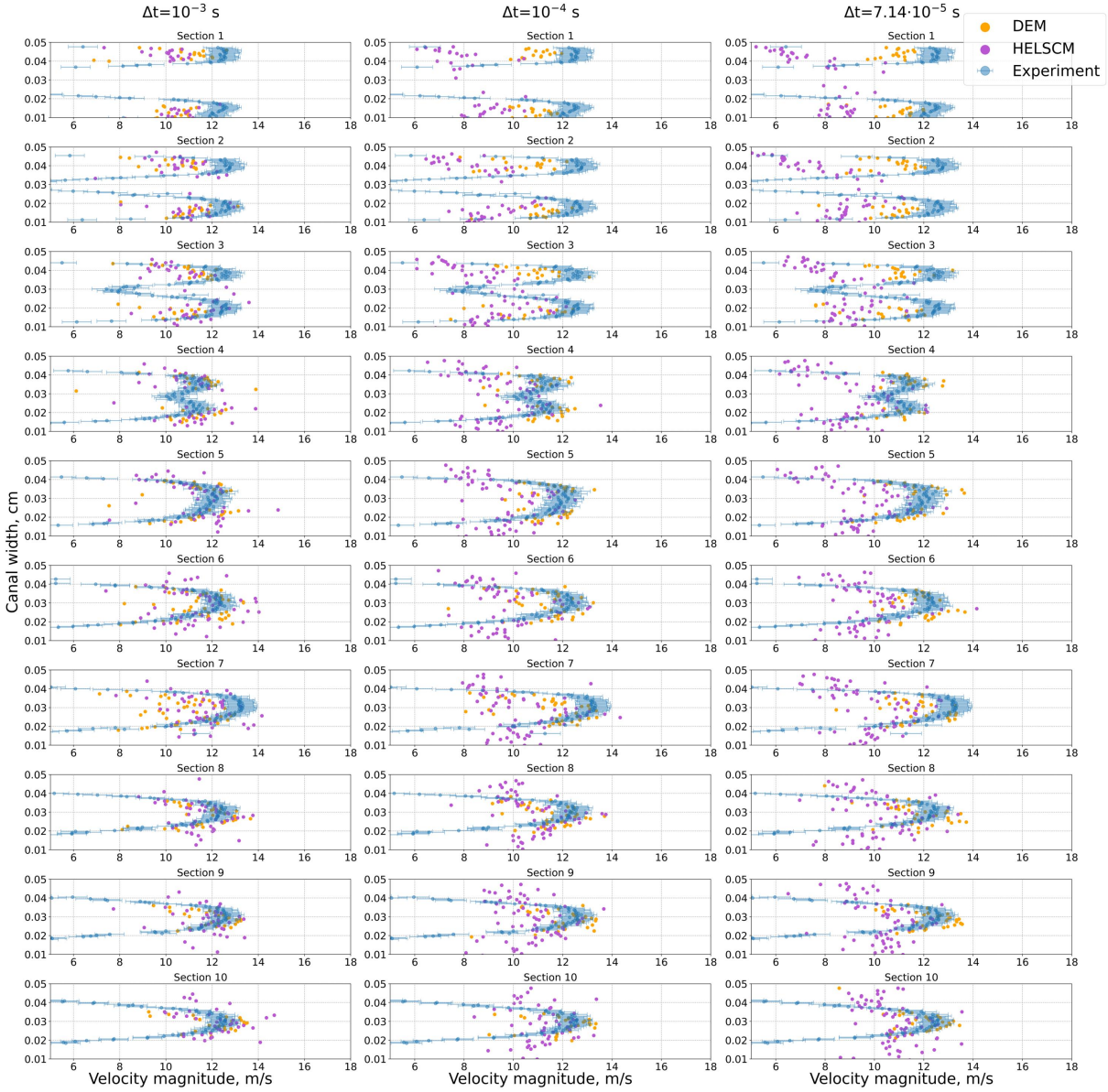

Figure 15: Quantitative comparison of the DEM and HELSCM model based on calculated particle velocity profiles, at ten location downstream of the computational domain (see Fig. 10), obtained for different time steps for particle size 315 μm after 0.02 seconds of numerical simulation and using 88 boxes for profiles reconstruction

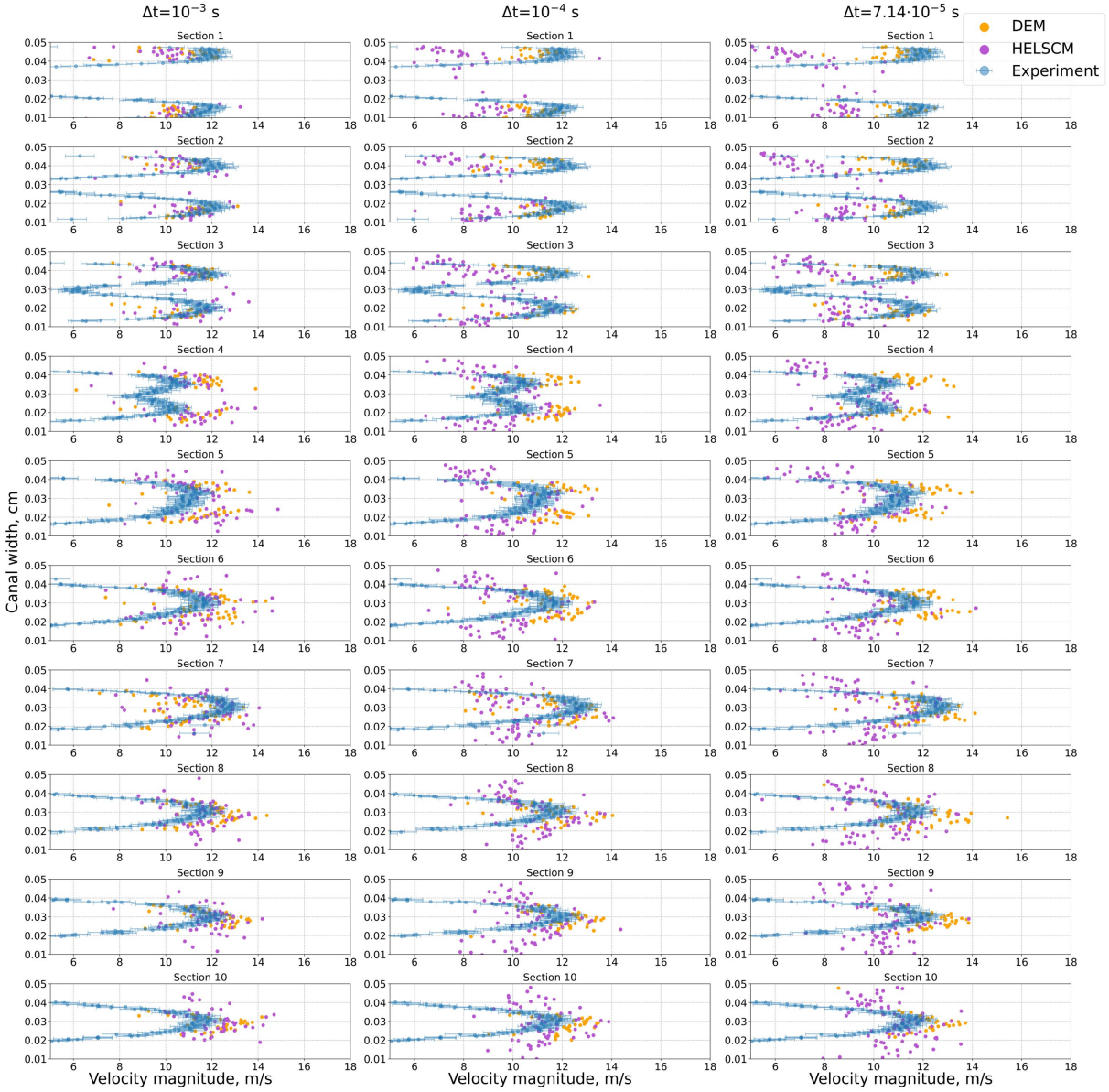

Figure 16: Quantitative comparison of the DEM and HELSCM model based on calculated particle velocity profiles, at ten locations downstream of the computational domain (see Fig. 10), obtained for different time steps for particle size 315 μm after 0.02 seconds of numerical simulation and using 126 boxes for profile reconstruction

It can be seen that with the decrease of the simulation time step, larger differences in numerical results contrary to the experimental data can be noticed. The largest discrepancies can be observed for subboxes resolution 20 and at velocity profiles calculated at three rear locations for time steps 10^{-4} s and $7.14 \cdot 10^{-5}$ s. With decreasing the time step for the HELSCM approach, the particle collision rate increases, which consequently affects the distribution of the particles as illustrated in figure 17 (upper rows). The particle dispersion effect can also be observed in Figure 17 (lower rows), which illustrates the distribution of the solid volume fraction in logarithmic scale obtained after 0.02 seconds of wall clock simulation time. The currently used implementation of the surrogate collision model (SCM) in the HEL approach did not take into account the particle contact time. The small time step causes multiple detections of the same colliding particle. This provides a perturbation to the predicted particle velocity and, in consequence, their trajectories due to the number of calls of the collision model. In

summary, multiple detection affects the dispersion of the particles in the computational domain as depicted in figure 17 (upper rows).

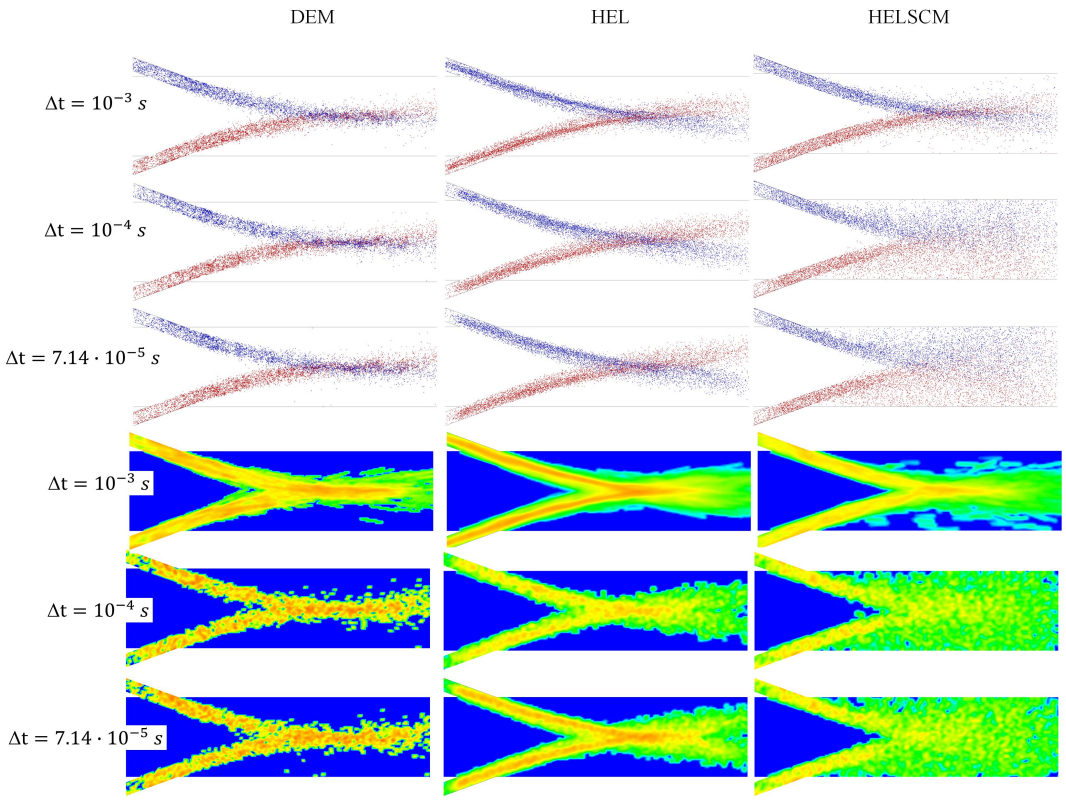

Figure 17: Qualitative comparison of the DEM and HELSCM models based the particle dispersion (upper row) and contours of the solid phase distribution on logarithmic scale (lower row), calculated for different time steps carried out for particle size 315 μm after 0.02 seconds of numerical simulation

To improve the implementation of HELSCM, the particle collision rate between the same particles must be tracked. However, this will lead to an extension of the execution time. In the tests carried out, the balance between execution time and accuracy was sought. To decrease the simulation time, some simplifications were necessary to be introduced into the model. Using an additional procedure can lead to extension execution time, where it can be close to DEM.

The smallest discrepancies between the experimental and numerical results can be seen for simulations, running with a time step equal to 10^{-3} s. It can be observed for the results obtained using both numerical models within the ten locations. Figure 16 shows that the DEM approach returns higher velocities in the center of the computational domain. By application of the DEM approach, the effect of particle dispersion is attenuated and the particles after collision are mostly concentrated in the center of computational domain, which can be noticed also in figure 17 (lower row). The qualitative comparison of the particle distributions obtained from the experiment and the numerical simulation carried out using the DEM and HELSCM approach is shown in figure 18. It can be seen that for simulation run for the smallest time step using both numerical approaches, the experimentally determined particle distribution is between the DEM and HELSCM results.

The most comparable results, qualitatively and quantitatively, were achieved using the HELSCM approach and using the longest time step (0.001 seconds). Figure 17 also shows the numerical results obtained using the standard hybrid Euler-Lagrnage approach. It can be easily seen that, in given volume fractions of solid material in the computational domain, the KTGF model is unable to track the mutual interactions between the particles. For the three investigated time steps, both particle streams pass each other without interactions. Figures 17 illustrate

that qualitatively the particle distribution obtained from the HEL simulation looks very similar to the experimental one, as can be seen in figure 18. Nevertheless, there were no collisions between two colliding particle streams regardless of the simulation time step taken.

Based on the study carried out, it can be concluded that the objective of this work was achieved. The intention of introducing a new collision model, developed based on the machine learning technique, was to increase the accuracy of the standard HEL model in collision detection, while not increasing the simulation time. Figure 22 shows that the simulation time applying the HELSCM is comparable to the standard HEL model for three investigated time steps. Relatively large time step, as that typically used in modeling multiphase flows of 10^{-3} seconds, the collision effect is easily observed by application of the HELSCM, which cannot be observed in standard HEL approach.

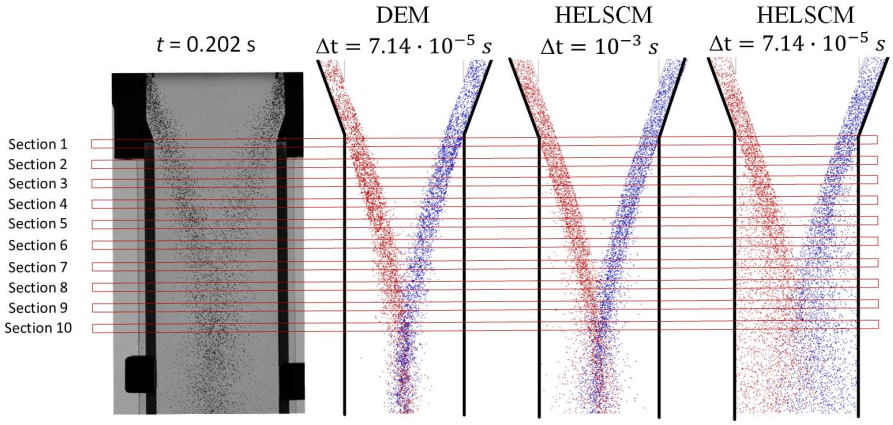

Figure 18: Comparison of numerical results with experimental data based on particle dispersion in the computational domain determined after 0.03 seconds of wall clock time of numerical simulations using DEM and developed HELSCM approaches for particle size 315 μm and marked locations used for the determination of particle velocity profiles.

For particle mean diameter 475 μm the quantitative model comparison was carried out only using the highest resolution of the velocity profile, that is, using 126 sub-boxes and three earlier mentioned simulation time steps. Figure 19 shows the calculated velocity profiles for three investigated time steps compared to the experimental data. The largest discrepancies between the experimental and numerical results can be seen in the rear locations of the ten investigated positions. The most comparable results can be indicated for simulation time steps equal to 0.001 s, as was also observed for a particle mean size equal to 315 μm. The largest discrepancies can be observed for the calculated profiles for the three posterior locations. Nevertheless, it can be seen that particle velocity profiles at the last two locations evidently decrease in contrast to the eight remaining locations. Due to the shifting of the two streams, the collision region is closer to the inlets, which is an opposite situation in comparison to the smaller particle diameter. As a consequence, colliding particles cause an intensive dispersion of particles at locations placed downstream from inlets, which can be seen in figure 21. By frame-by-frame analysis of the experimental data, it was observed that part of the colliding particles change trajectories and move upstream or perpendicularly to the flow direction. For both cases considered in this paper, the calculated Stokes number (St= t_F/t_{RT}) for a given flow condition was greater than the unit. The characteristic time of the flow field (t_F) was calculated taking into account the relationship between the area of the channel cross section and its perimeter and the mean velocity of air in the considered channel. The diameter of the particle affects the response time (t_{RT}), which for the mean particle diameter 475 μm ($t_{RT} = 0.25$ s) was almost twice as high compared to the response time calculated for particle mean diameter 315 μm ($t_{RT} = 0.13$ s). Here, the particle response time was calculated by solving the simplified equation of motion (4) for a single particle (the terms ∇/ρ_p and F_{coll} are neglected). Due to the large values of the Stokes number (St) in the case of sudden change of the particle direction, it takes a while before the particle velocity stabilizes. The algorithm used to identify particle velocity profiles [41] tracks only particles that move in the downstream direction along the flow and consequently affect the determined velocity profiles.

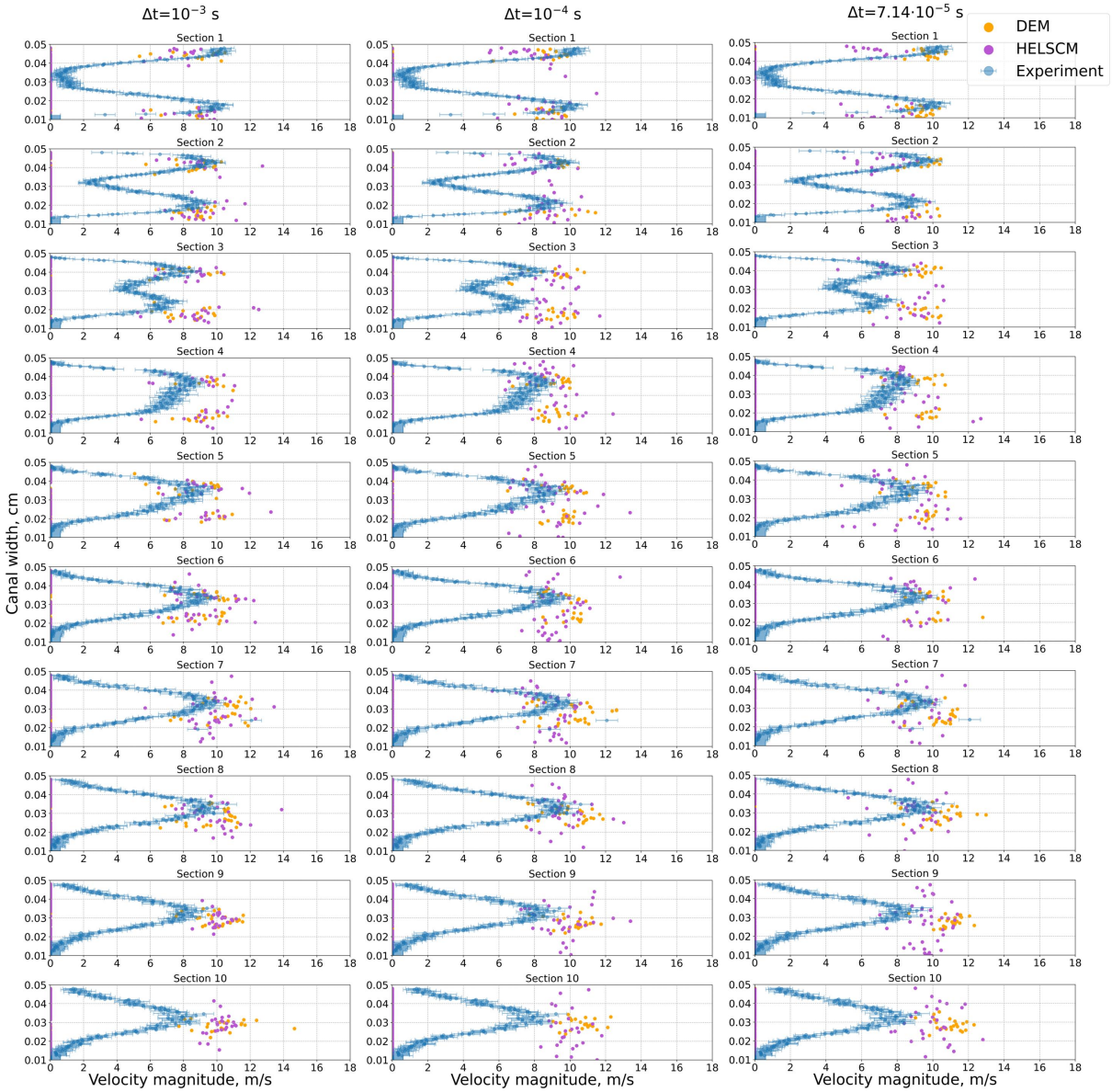

Figure 19: Quantitative comparison of the DEM and HELSCM model, based on calculated time average particle velocity profiles, at ten locations downstream of the computational domain (see Fig. 10), obtained for different time steps for particle size 475 μm after 0.02 seconds of numerical simulation

Figure 20 illustrates the particle distribution and contours of the solid volume fraction calculated after 0.02 seconds of simulation. In the case of the DEM application, the particles were mostly tracked in the center of the computational domain and observed for three investigated time steps. However, as illustrated in figure 21 where the DEM results were compared with the experimental data, the DEM results show a smaller dispersion of particles. An opposite effect in the collision region can be observed for numerical results obtained by the application standard HEL model for investigated particle diameters. Figures 20 show that in the investigated configuration of the numerical model and the solid volume fraction used the collision effect cannot be observed for both particle diameters. The HEL approach is not sensitive to particle diameter.

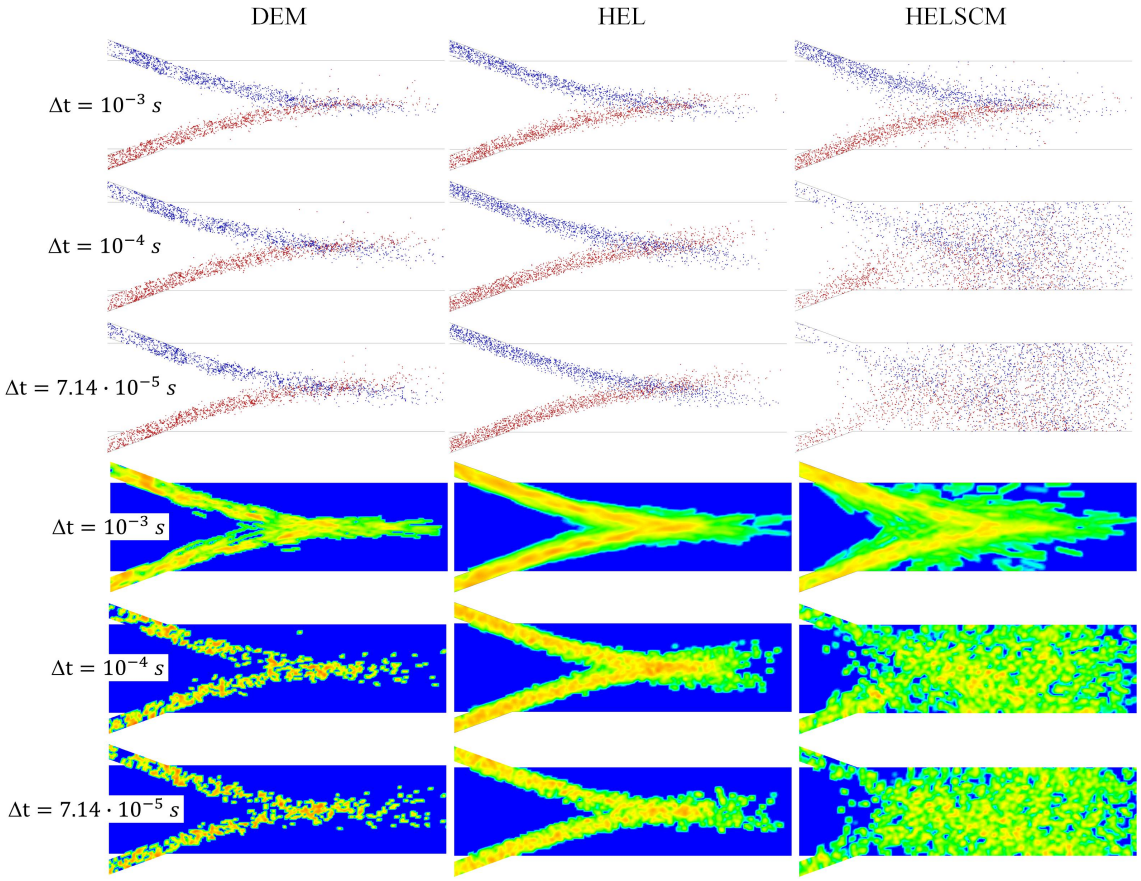

Figure 20: Qualitative comparison of the DEM and HELSCM models based on particle dispersion (upper row) and contours of the solid phase distribution on logarithmic scale (lower row), calculated for different time steps carried out for particle size 475 μm after 0.02 seconds of numerical simulation

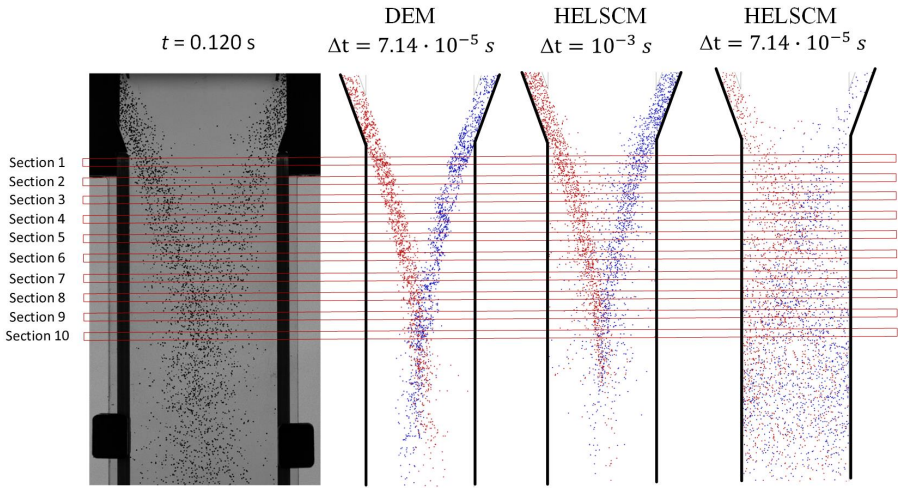

Figure 21: Qualitative comparison of numerical results against experimental data based on particle dispersion in the computational domain determined after 0.02 seconds of wall clock time of numerical simulations using DEM and developed HELSCM approaches for particle size 475 μm

Figure 22 shows the comparison of execution times for three, here investigated time steps ($\Delta t = 10^{-3}$ s, 10^{-4} s and $7.14 \cdot 10^{-5}$ s), three models used (DEM, HEL and HELSCM) and two particle sizes (315 μm and 475 μm). It can be clearly seen that the application of new collision model gives a possibility to considerably reduce computational time, in contrary to the standard DEM approach. Using the HELSCM model, the simulation time is comparable to the standard HEL approach, which confirms that the goal of this work was reached, also taking into account the qualitative and quantitative comparison. An additional conclusion can be formulated by comparing the simulation time for two particle diameters used. The number of tracked particles for two particle sizes differ, so the simulation time for used larger particles was shorter because the number of detected collisions in subsequent time steps is smaller. This affects the simulation time, because the predictive model was not called so many times as for case with smaller particle size where the number of particles was almost 3.5 larger. This can be seen in figure 23, which shows the collision rate for three investigated time steps, and two particle diameters considered in this work.

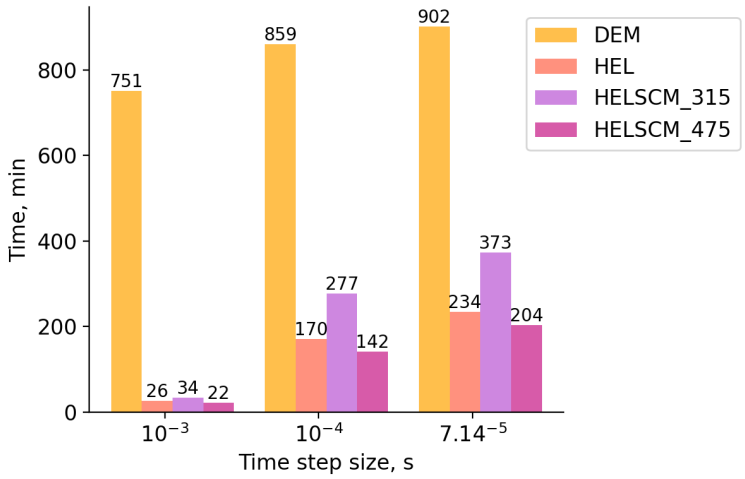

Figure 22: Comparison of DEM and HELSCM execution times, carried out using a single process at the same work station

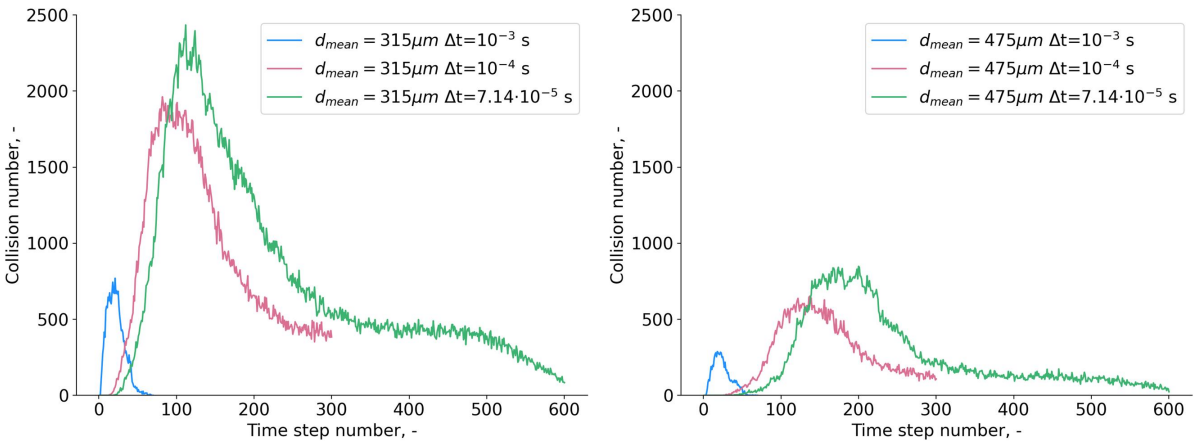

Figure 23: Comparison of collision rates calculated for three investigated time steps of numerical simulations and two used particle diameters

9. Summary

The presented work focused on development of new collision model that can be used as an alternative to standard collision models developed within the framework of the Kinetic Theory of Granular Flow (KTGF). Main attention was paid to improved functionality of the standard hybrid Eulerian-Lagrangian (HEL) approach, which is frequently used for modeling dense granular flow on laboratory and industrial scales. The main advantage of the HEL technique is the cost of numerical simulation, which is considerably lower, even by a few orders of magnitude, contrary to the Discrete Element Method (DEM). The main difference, between motioned here techniques, lies in the way in which the collisions are detected. Using the HEL approach, the collision forces acting on the particles are determined on the basis of the volume fraction of the solid material in the computational cell, according to the mentioned KTGF theory. It is straightforward that the accuracy of the HEL approach is directly related to the resolution of the mesh. Furthermore, the distribution of the solid volume fraction also affects the closure of the KTGF approach models that has an impact on the solution. In the case of modeling dilute systems, the collision effect can be difficult to observe in the case of application of the HEL approach.

Knowing the basic limitations of both mentioned approaches, which can be used for modeling dense granular flows, it is straightforward that there is a real need of development of the model that can combine aforementioned advantages of each model. This work provides an answer to the formulated question, i.e. how the accurate DEM collision model can be combined with the simple HEL technique to increase its accuracy, in collision detection, and in the same time not increase the cost of numerical simulation.

To achieve this goal, the novel collision model, i.e. the hybrid Eulerian-Lagrangian Surrogate Collision Model (HELSCM), was proposed in terms of the application of the machine learning (ML) technique. In the discussed procedure, the XGBoost, decision trees, and gradient boosting technique was used to determine the relationships between input data (features) and output data (target). For validation of the functionality of the developed HELSCM approach, the numerical results obtained for two particle diameters 315 μm and 475 μm and three investigated simulation time steps $\Delta t = 10^{-3}$ s, 10^{-4} s and $7.14 \cdot 10^{-5}$ s were compared against the experimental data. It was done quantitatively by comparison of the solid velocity profiles obtained from carried out experimental work, taking into account the source of error that comes from carried out experiments.

The experiment study and subsequent analysis allowed us to draw conclusions from the developed methodology, which are highlighted below. On the basis of the tests carried out, it was clearly seen that the application of the HELSCM model gives the possibility to considerably reduce computational time, contrary to the standard DEM approach. Using the HELSCM model, the simulation time was comparable to the standard HEL approach. The advantages of the introduced here methodology for modeling collisions are the possibility of performing multiphase simulation with a time step of order $\Delta t = 10^{-3}$ s with an accuracy of the DEM. In case of the usage of standard DEM, the simulation time step is a function of the flow conditions, particle size, and can be even smaller than $\Delta t = 10^{-5}$ s. In such a case, the simulation time can be considerably higher than that achieved by applying the developed HELSCM model, which was also demonstrated in this study. The carried out work shows also that with decreasing of the simulation time step for HELSCM, the larger differences in numerical results were noticed. With decreasing the time step, the particle collision rate increased, which in consequence affected the distribution of the particles within the computational domain. The used implementation of the HELSCM did not take into account the particle contact time. This means that in case of small time step a multiple collision between particles can be observed which introduced additional error to the final velocity components. The most comparable results, both qualitatively and quantitatively were reached using HELSCM approach using largest time step ($\Delta t = 10^{-3}$).

To summarize the work presented, it can be concluded that the formulated requirements for the novel collision model were finally reached. By application of HELSCM, results comparable to the experimental and DEM data were achieved for a large time step. It can be said that the HELSCM technique has accuracy of the DEM, while the execution time was considerably reduced. As each model has some drawbacks, also HELSCM is not perfect for all application and still intensive research is required. As an example, the detection of the collision, here the distance between particles, was used. In case of application for larger systems, it need to be changed to particle detection in computational cell. Undoubtedly, such an approach will be sensitive to the mesh resolution, while it is worth to check, because it is expected that simulation time will decrees. Furthermore, the functionality of developed in this paper strategy should be investigated in case of its application for modeling small lab scale

circulating fluidized bed (CFB) installation. Here, only monodisperse systems were investigated. Nevertheless, in future research it is required to take into account the polydisperse system, where different configurations of particle distribution will be investigated. Initially, the mixture of two particle diameters that were investigated in this work can be used.

Acknowledgments

This research was supported by the National Science Center within the OPUS scheme under contract 2018/31/B/ST8/02201.

References

[1] Besedina, Skverchinskaya, Shmakov, et al., Persistent red blood cells retain their ability to move in microcapillaries under high levels of oxidative stress, Communications Biology 5 (2022). doi:https://doi.org/10.1038/s42003-022-03620-5.

[2] M. Gracka, R. Lima, J. M. Miranda, S. Student, B. Melka, Z. Ostrowski, Red blood cells tracking and cell-free layer formation in a microchannel with hyperbolic contraction: A cfd model validation, Computer Methods and Programs in Biomedicine 226 (2022) 107117. doi:https://doi.org/10.1016/j.cmpb.2022.107117.
URL https://www.sciencedirect.com/science/article/pii/S0169260722004989

[3] Fluidized particles. by j. f. davidson and d. harrison. cambridge university press, 1963. 155 pp. 35s., volume=33, doi=10.1017/S0022112068221560, number=3, journal=Journal of Fluid Mechanics, publisher=Cambridge University Press, author=Pigford, R. L., year=1968, pages=623–624.

[4] H. Flood, Fluidized bed drying of food: A new development in the drying, roasting, cooking and freezing of food, Cornell Hotel and Restaurant Administration Quarterly 5 (1) (1964) 65–70. arXiv:https://doi.org/10.1177/001088046400500115, doi:10.1177/001088046400500115.
URL https://doi.org/10.1177/001088046400500115

[5] R. Arévalo, I. Zuriguel, Clogging of granular materials in silos: effect of gravity and outlet size, Soft Matter 12 (2016) 123–130. doi:10.1039/C5SM01599E.
URL http://dx.doi.org/10.1039/C5SM01599E

[6] R. Greve, K. Hutter, Motion of a granular avalanche in a convex and concave curved chute: experiments and theoretical predictions, Philosophical Transactions of the Royal Society of London. Series A: Physical and Engineering Sciences 342 (1666) (1993) 573–600. arXiv:https://royalsocietypublishing.org/doi/pdf/10.1098/rsta.1993.0033, doi:10.1098/rsta.1993.0033.
URL https://royalsocietypublishing.org/doi/abs/10.1098/rsta.1993.0033

[7] P. Jop, Y. Forterre, O. Pouliquen, A constitutive law for dense granular flows, Nature 441 (2006). doi:https://doi.org/10.1038/nature04801.

[8] R. Camassa, D. Harris, R. Hunt, Z. Kilic, R. McLaughlin, A constitutive law for dense granular flows, Nat Commun 10 (2019). doi:https://doi.org/10.1038/s41467-019-13643-y.

[9] U. Khadka, V. Holubec, H. Yang, F. Cichos, Active particles bound by information flows, Nature Communications 9 (2018). doi:https://doi.org/10.1038/s41467-018-06445-1.

[10] Y. Jiang, G. Qiu, H. Wang, Modelling and experimental investigation of the full-loop gas–solid flow in a circulating fluidized bed with six cyclone separators, Chemical Engineering Science 109 (2014) 85–97.

[11] S. Shah, K. Myöhänen, S. Kallio, T. Hyppänen, CFD simulations of gas-solid flow in an industrial-scale circulating fluidized bed furnace using subgrid-scale drag models, Particuology 18 (2015) 66–75.

[12] W.P. Adamczyk, Application of the Numerical Techniques for Modelling Fluidization Process Within Industrial Scale Boilers, Archives of Computational Methods in Engineering 10 (2016) 1–34.

[13] X. Shi, X. Lan, F. Liu, Y. Zhang, J. Gao, Effect of particle size distribution on hydrodynamics and solids back-mixing in cfb risers using cpfd simulation, Powder Technology 266 (2014) 135 – 143.

[14] S. Kraft, F. Kirnbauer, H. Hofbauer, Cpfd simulations of an industrial-sized dual fluidized bed steam gasification system of biomass with 8mw fuel input, Applied Energy 190 (2017) 408 – 420.

[15] M. Farid, H. Jeong, K. Kim, J. Lee, D. Kim, J. Hwang, Numerical investigation of particle transport hydrodynamics and coal combustion in an industrial-scale circulating fluidized bed combustor: Effects of coal feeder positions and coal feeding rates, Fuel 192 (2017) 187–202.

[16] C. Crowe, J. Schwarzkopf, M. Sommerfeld, Y. Tsuji, Multiphase flows with droplets and particles, Taylor & Francis Group, 2012.

[17] J. Lin, K. Luo, S. Wang, C. Hu, J. Fan, An augmented coarse-grained cfd-dem approach for simulation of fluidized beds, Advanced Powder Technology 31 (10) (2020) 4420 – 4427.

[18] T. Tsuji, K. Yabumoto, T. Tanaka, Spontaneous structures in three-dimensional bubbling gas-fluidized bed by parallel DEM-CFD coupling simulation, Powder Technology 184 (2008) 132–140.

[19] J. D. D., Gidaspow, A bubbling fluidization model using kinetic theory of granular flow, AIChE Journal 36 (1) (1990) 523–532.

[20] D. Gidaspow, Multiphase Flow and Fluidization, Academic Press, Boston, MA., 1994, reaction Engineering International.

[21] P. Adesina, C. O'Sullivan, T. Morimoto, M. Otsubo, Determining a representative element volume for dem simulations of samples with non-circular particles, Particuology 68 (2022) 29–43. doi:https://doi.org/10.1016/j.partic.2021.10.007.
URL https://www.sciencedirect.com/science/article/pii/S1674200121002169

[22] A. Busch, S. T. Johansen, On the validity of the two-fluid-ktgf approach for dense gravity-driven granular flows as implemented in ansys fluent r17.2, Powder Technology 364 (2020) 429–456. doi:https://doi.org/10.1016/j.powtec.2020.01.043.
URL https://www.sciencedirect.com/science/article/pii/S003259102030053X

[23] N. Ahmad, Y. Tian, B. Lu, K. Hong, H. Wang, W. Wang, Extending the emms/bubbling model to fluidization of binary particle mixture: Formulation and steady-state validation, Chinese Journal of Chemical Engineering 27 (1) (2019) 54–62. doi:https://doi.org/10.1016/j.cjche.2018.04.011.
URL https://www.sciencedirect.com/science/article/pii/S1004954118300879
[24] L. Zhang, J. Chen, W. Huang, J. Li, A direct solution to multi-objective optimization: Validation in solving the emms model for gas-solid fluidization, Chemical Engineering Science 192 (2018) 499–506. doi:https://doi.org/10.1016/j.ces.2018.07.033.
URL https://www.sciencedirect.com/science/article/pii/S0009250918305001
[25] A. Ullah, I. Jamil, A. Hamid, K. Hong, Emms mixture model with size distribution for two-fluid simulation of riser flows, Particuology 38 (2018) 165–173. doi:https://doi.org/10.1016/j.partic.2017.06.007.
URL https://www.sciencedirect.com/science/article/pii/S1674200117301517
[26] Z. Wang, C. Liu, L. Wang, S. Yin, L. Tong, Dust distribution of solid and adhesive mixed dust in a granular bed filter, Particuology 67 (2022) 1–7. doi:https://doi.org/10.1016/j.partic.2021.09.008.
URL https://www.sciencedirect.com/science/article/pii/S1674200121001917
[27] Y. Liang, Y. Zhang, T. Li, C. Lu, A critical validation study on cpfd model in simulating gas–solid bubbling fluidized beds, Powder Technology 263 (2014) 121–134. doi:https://doi.org/10.1016/j.powtec.2014.05.003.
URL https://www.sciencedirect.com/science/article/pii/S0032591014004367
[28] V. Patel, M. Shah, A comprehensive study on artificial intelligence and machine learning in drug discovery and drug development, Intelligent Medicine (2021). doi:https://doi.org/10.1016/j.imed.2021.10.001.
URL https://www.sciencedirect.com/science/article/pii/S2667102621001066
[29] X. Lang, D. Wu, W. Mao, Comparison of supervised machine learning methods to predict ship propulsion power at sea, Ocean Engineering 245 (2022) 110387. doi:https://doi.org/10.1016/j.oceaneng.2021.110387.
URL https://www.sciencedirect.com/science/article/pii/S0029801821016802
[30] L. Zhou, Y. Song, W. Ji, H. Wei, Machine learning for combustion, Energy and AI 7 (2022) 100128. doi:https://doi.org/10.1016/j.egyai.2021.100128.
URL https://www.sciencedirect.com/science/article/pii/S2666546821000756
[31] J. Grochowalski, P. Jachymek, M. Andrzejczyk, M. Klajny, A. Widuch, P. Morkisz, B. Hernik, J. Zdeb, W. Adamczyk, Towards application of machine learning algorithms for prediction temperature distribution within cfb boiler based on specified operating conditions, Energy 237 (2021) 121538. doi:https://doi.org/10.1016/j.energy.2021.121538.
URL https://www.sciencedirect.com/science/article/pii/S0360544221017862
[32] N. S. Mohd Yahya, L. Y. Ng, V. Andiappan, Optimisation and planning of biomass supply chain for new and existing power plants based on carbon reduction targets, Energy 237 (2021) 121488. doi:https://doi.org/10.1016/j.energy.2021.121488.
URL https://www.sciencedirect.com/science/article/pii/S0360544221017369
[33] W. Chen, B. Zhou, H. Huang, Y. Lu, S. Li, F. Gao, Design, modeling and performance analysis of a deployable wec for ocean robots, Applied Energy 327 (2022) 119993. doi:https://doi.org/10.1016/j.apenergy.2022.119993.
URL https://www.sciencedirect.com/science/article/pii/S0306261922012508
[34] M. Goldsworthy, T. Moore, M. Peristy, M. Grimeland, Cloud-based model-predictive-control of a battery storage system at a commercial site, Applied Energy 327 (2022) 120038. doi:https://doi.org/10.1016/j.apenergy.2022.120038.
URL https://www.sciencedirect.com/science/article/pii/S0306261922012958
[35] H.-H. Tsao, Y.-G. Leu, L.-F. Chou, A center-of-concentrated-based prediction interval for wind power forecasting, Energy 237 (2021) 121467. doi:https://doi.org/10.1016/j.energy.2021.121467.
URL https://www.sciencedirect.com/science/article/pii/S0360544221017151
[36] G. Li, S. Yin, H. Yang, A novel crude oil prices forecasting model based on secondary decomposition, Energy 257 (2022) 124684. doi:https://doi.org/10.1016/j.energy.2022.124684.
URL https://www.sciencedirect.com/science/article/pii/S0360544222015870
[37] T. Fang, C. Zheng, D. Wang, Forecasting the crude oil prices with an emd-isbm-fnn model, Energy 263 (2023) 125407. doi:https://doi.org/10.1016/j.energy.2022.125407.
URL https://www.sciencedirect.com/science/article/pii/S0360544222022897
[38] W. Chen, Q. Wang, J. S. Hesthaven, C. Zhang, Physics-informed machine learning for reduced-order modeling of nonlinear problems, Journal of Computational Physics 446 (2021) 110666. doi:https://doi.org/10.1016/j.jcp.2021.110666.
URL https://www.sciencedirect.com/science/article/pii/S0021999121005611
[39] G. Aversano, M. Ferrarotti, A. Parente, Digital twin of a combustion furnace operating in flameless conditions: reduced-order model development from cfd simulations, Proceedings of the Combustion Institute 38 (4) (2021) 5373–5381. doi:https://doi.org/10.1016/j.proci.2020.06.045.
URL https://www.sciencedirect.com/science/article/pii/S1540748920300742
[40] H. Wang, Z. Li, N. Cai, Reduced-order model for redox kinetics of oxygen carrier in chemical looping combustion, Proceedings of the Combustion Institute 38 (4) (2021) 5271–5279. doi:https://doi.org/10.1016/j.proci.2020.08.002.
URL https://www.sciencedirect.com/science/article/pii/S1540748920303011
[41] A. Widuch, K. Myöhänen, M. Nikku, M. Nowak, A. Klimanek, W. Adamczyk, Data set generation at novel test-rig for validation of numerical models for modeling granular flows, International Journal of Multiphase Flow 142 (2021) 103696. doi:https://doi.org/10.1016/j.ijmultiphaseflow.2021.103696.
URL https://www.sciencedirect.com/science/article/pii/S0301932221001440
[42] Bronkhorst high-tech b.v.
URL https://www.bronkhorst.com/int/
[43] Vision research, inc.
URL https://www.phantomhighspeed.com/products/cameras/veo/veo710

[44] NI LabVIEW, National Instruments Corp., http://www.ni.com.
[45] Cospheric llc.
URL https://www.cospheric.com
[46] H. Ku, Notes on the use of propagation of error formulas, JOURNAL OF RESEARCH of the National Bureau of Standards - C. Engineering and Instrumentation 70C (4) (1966) 263–273.
[47] R. S., M. K., H. T., Modeling the behavior of limestone particles in oxy-fuel CFB processes, Fuel 127 (2014) 141–150.
[48] F. Alobaid, N. Almohammed, M. Massoudi Farid, J. May, P. Rößger, A. Richter, B. Epple, Progress in cfd simulations of fluidized beds for chemical and energy process engineering, Progress in Energy and Combustion Science (2021) 100930doi:https://doi.org/10.1016/j.pecs.2021.100930.
URL https://www.sciencedirect.com/science/article/pii/S0360128521000289
[49] T. Dymala, T. Wytrwat, S. Heinrich, Mp-pic simulation of circulating fluidized beds using an emms based drag model for geldart b particles, Particuology 59 (2021) 76–90, towards Modelling Solids and Multiphase Flow for Large Scale Industrial Systems and Applications. doi:https://doi.org/10.1016/j.partic.2021.07.002.
URL https://www.sciencedirect.com/science/article/pii/S1674200121001334
[50] S. Rostom, H. de Lasa, Downer fluidized bed reactor modeling for catalytic propane oxidative dehydrogenation with high propylene selectivity, Chemical Engineering and Processing - Process Intensification 137 (2019) 87–99. doi:https://doi.org/10.1016/j.cep.2019.02.002.
URL https://www.sciencedirect.com/science/article/pii/S0255270118313643
[51] S. Wang, K. Luo, C. Hu, J. Lin, J. Fan, Cfd-dem simulation of heat transfer in fluidized beds: Model verification, validation, and application, Chemical Engineering Science 197 (2019) 280–295. doi:https://doi.org/10.1016/j.ces.2018.12.031.
URL https://www.sciencedirect.com/science/article/pii/S0009250919300041
[52] V. Jain, L. Kalo, D. Kumar, H. J. Pant, R. K. Upadhyay, Experimental and numerical investigation of liquid–solid binary fluidized beds: Radioactive particle tracking technique and dense discrete phase model simulations, Particuology 33 (2017) 112–122.
[53] S. Cloete, S. T. Johansen, S. Amini, Performance evaluation of a complete lagrangian ktgf approach for dilute granular flow modelling, Powder Technology 226 (2012) 43–52.
[54] D. J., L. R.W, Three-dimensional kinetic theory modelling of hydrodynamics and erosion in fluidized bed, Powder Technology 73 (1992) 127–138.
[55] K. Myöhänen, T. Hyppänen, A three-dimensional model frame for modelling combustion and gasification in circulating fluidized bed furnaces, International Journal Of Chemical Reactor Engineering 9 (2011) A25.
[56] O. T. Sreekanth P., Syamlal M., Computational gas-solids flows and reacting systems: theory, methods and practice, Engineering Science Reference IGI Global, 2012, iSBN 978-1-61520-651-2.
[57] C. Crowe, J. Schwarzkopf, M. Sommerfeld, Y. Tsuji, Multiphase flows with droplets and particles, Taylor & Francis Group, 2012, iSBN: 978-1-439-84050-4.
[58] H. Zhou, G. Flamant, D. Gauthier, J. Lu, Lagrangian approach for simulating the gas-particle flow structure in a circulating fluidized bed riser, International Journal of Multiphase Flow 28 (2002) 1801–1821.
[59] ANSYS Fluent Theory Guide, 2019R1.
[60] C. Lun, S. Savage, D. Jeffrey, N. Chepurnly, Kinetic theories for granular flow: inelastic particles in couette flow and slightly inelastic particles in a general flow field, Journal of Fluid Mechanics 140 (1984) 223–256.
[61] M. Syamlal, W. Rogers, T. O'Brien, MFIX Documentation, Theory Guide, National Technical Information Service 1 (1993) 5540–5551.
[62] A. Jensen, K. Fraser, G. Laird, Improving the precision of discrete element simulations through calibration models, 2014.
[63] C. Kloss, C. Goniva, LIGGGHTS – Open Source Discrete Element Simulations of Granular Materials Based on Lammps, John Wiley Sons, Ltd, 2011, pp. 781–788.
[64] J. Wang, H. Teng, Z. Han, M. R. Jensen, Discrete Element Method in LS-DYNA (DEM), Livermore (11 2012).
[65] T. Chen, C. Guestrin, Xgboost: A scalable tree boosting system, CoRR abs/1603.02754 (2016). arXiv:1603.02754.
URL http://arxiv.org/abs/1603.02754
[66] K. G. Robinson, R. E. Akins, Chapter 24 - machine learning in epigenetic diseases, in: T. O. Tollefsbol (Ed.), Medical Epigenetics (Second Edition), second edition Edition, Vol. 29 of Translational Epigenetics, Academic Press, 2021, pp. 513–525. doi:https://doi.org/10.1016/B978-0-12-823928-5.00038-4.
URL https://www.sciencedirect.com/science/article/pii/B9780128239285000384
[67] J. R. Quinlan, Induction of decision trees, Machine Learning 1 (1986) 81–106.
[68] J. H. Friedman, Greedy function approximation: A gradient boosting machine., The Annals of Statistics 29 (5) (2001) 1189 – 1232. doi:10.1214/aos/1013203451.
URL https://doi.org/10.1214/aos/1013203451
[69] S. Rong, Z. Bao-wen, The research of regression model in machine learning field, MATEC Web of Conferences 176 (2018) 01033. doi:10.1051/matecconf/201817601033.
[70] E. Eyo, S. Abbey, Machine learning regression and classification algorithms utilised for strength prediction of opc/by-product materials improved soils, Construction and Building Materials 284 (2021) 122817. doi:https://doi.org/10.1016/j.conbuildmat.2021.122817.
URL https://www.sciencedirect.com/science/article/pii/S0950061821005778
[71] C. C.L, J. D.S, S. Sonoli, Multiple linear regression analysis for prediction of boiler losses and boiler efficiency, International Journal of Instrumentation and Control Systems 8 (2018) 01–09. doi:10.5121/ijics.2018.8201.
[72] Coadou, Yann, Boosted decision trees and applications, EPJ Web of Conferences 55 (2013) 02004. doi:10.1051/epjconf/20135502004.
URL https://doi.org/10.1051/epjconf/20135502004
[73] T. Chen, C. Guestrin, Xgboost: A scalable tree boosting system, in: Proceedings of the 22nd ACM SIGKDD International Conference

on Knowledge Discovery and Data Mining, KDD '16, Association for Computing Machinery, New York, NY, USA, 2016, p. 785–794. doi:10.1145/2939672.2939785.
URL https://doi.org/10.1145/2939672.2939785
[74] P. Cundall, O. Strack, A discrete element model for granular assemblies, Géotechnique, 1979.
[75] J. D. Miller, Statistics for Data Science, Packt Publishing, 2017.
[76] P. Muhammad Ali, R. Faraj, Data normalization and standardization: A technical report (01 2014). doi:10.13140/RG.2.2.28948.04489.
[77] M. Claesen, B. De Moor, Hyperparameter search in machine learning (2015). doi:10.48550/ARXIV.1502.02127.
URL https://arxiv.org/abs/1502.02127
[78] T. Akiba, S. Sano, T. Yanase, T. Ohta, M. Koyama, Optuna: A next-generation hyperparameter optimization framework, in: Proceedings of the 25th ACM SIGKDD international conference on knowledge discovery & data mining, 2019, pp. 2623–2631.
[79] A. Widuch, K. Myöhänen, M. Nikku, M. Nowak, A. Klimanek, W. Adamczyk, Towards application of uncertainty quantification procedure combined with experimental procedure for assessment of the accuracy of the dem approach, International Journal of Multiphase Flow 142 (2021) 103696. doi:https://doi.org/10.1016/j.ijmultiphaseflow.2021.103696.
URL https://www.sciencedirect.com/science/article/pii/S0301932221001440
[80] P. Cyklis, P. Młynarczyk, The influence of the spatial discretization methods on the nozzle impulse flow simulation results, Procedia Engineering 157 (2016) 396–403, selected Papers from IX International Conference on Computational Heat and Mass Transfer (IC-CHMT2016). doi:https://doi.org/10.1016/j.proeng.2016.08.382.
URL https://www.sciencedirect.com/science/article/pii/S1877705816325577
[81] S. Ogawa, A. Umemura, N. Oshima, On the Equation of Fully Fluidized Granular Materials, Journal of Applied Mathematics and Physics 31 (1980) 483–493.
[82] D. Schaeffer, Instability in the Evolution Equations Describing Incompressible Granular Flow, Journal of Differential Equation 66 (1987) 19–50.
[83] L. Huilin, D. Gidaspow, Hydrodynamics of binary fluidization in a riser: CFD simulation using two granular temperatures, Chemical Engineering Science 58 (2003) 3777–3792.
[84] X. Wang, F. Jiang, X. Xu, B. Fan, J. Lei, Y. Xiao, Experiment and CFD simulation of gas solid flow in the riser of dense fluidized bed at high gas velocity, Powder Technology 199 (2010) 203–212.